Computers and Chemical Engineering 183 (2024) 108586

Contents lists available at ScienceDirect

Computers and Chemical Engineering

journal homepage: www.elsevier.com/locate/compchemeng

Hybrid model development and nonlinear model predictive control implementation for continuous dry granulation process

Yan-Shu Huang [a,*], Rexonni B. Lagare [a], Phoebe Bailey [a], David Sixon [a], Marcial Gonzalez [b,c], Zoltan K. Nagy [a], Gintaras V. Reklaitis [a]

[a] Davidson School of Chemical Engineering, Purdue University, West Lafayette, IN 47907, USA
[b] School of Mechanical Engineering, Purdue University, West Lafayette, IN 47907, USA
[c] Ray W. Herrick Laboratories, Purdue University, West Lafayette, IN 47907, USA

ARTICLE INFO

Keywords:
Model predictive control
Process control
Pharmaceutical continuous manufacturing
Process analytical technology (PAT)
Hybrid model
Roller compactor

ABSTRACT

This study focuses on the development of a hybrid model to integrate roll compaction and ribbon milling operations to design and control a continuous dry granulation process. The proposed hybrid model has three features: (1) it compensates for underestimated roll gap measurements with knurled rolls, (2) it represents the bimodal size distribution of granules using five fitting parameters of the bimodal Weibull distribution instead of only using specific size percentiles, and (3) it considers the impact of rotor-screen gaps on granules. Furthermore, the hybrid model facilitates the implementation of nonlinear model predictive control in a roller compactor Alexanderwerk WP120. Compared to widely applied open-loop operations in the pharmaceutical industry, nonlinear model predictive control demonstrates better performance, indicated by lower integral absolute errors in controlling mass throughput and ribbon solid fraction, in which real-time measurements can be obtained using a near-infrared sensor and a novel spectra selection approach.

1. Introduction

The dry granulation process is one of the important methods used in the pharmaceutical industry for the production of solid dosage forms such as tablets, capsules, and sachets. This method is preferred over wet granulation when materials are sensitive to heat and moisture. In addition, dry granulation is often a better candidate for continuous manufacturing than wet granulation because of its faster process dynamics by virtue of not requiring the relatively slow drying step. The main unit operation in the dry granulation process is the roller compactor, which consists of two operations: (1) roll compaction in which powder blends are compressed between two counter-rotating rolls to form a ribbon, and (2) ribbon milling in which ribbons are converted into granules.

The performance of the dry granulation process is determined by the intermediate ribbon properties and final granule properties. The advantages of dry granulation include enhancing blend uniformity and flowability by enlargement of particle size. Powder flowability plays an essential role in influencing the performance of the tablet manufacturing process and final drug product quality. For example, improvement of powder flowability can enhance the performance of die filling in the tableting process and reduce variability in tablet weight (Van Snick et al., 2018). Also, good powder flowability can reduce probe fouling and enhance the performance of on-line process analytical technology (PAT) tools, such as capacitance-based particulate flow rate sensor (Huang et al., 2022a) and widely applied near-infrared (NIR) spectroscopy-based composition sensors (Fonteyne et al., 2015). However, particle size over-enlargement or over-compression of powders can compromise the tabletability because of reduced bonding areas or granule hardening (also known as work hardening) (Herting and Kleinebudde, 2008; Sun and Kleinebudde, 2016). Finding the optimal balance between improving powder flowability and sacrificing powder tabletability, which are highly affected by ribbon solid fraction (also known as relative ribbon density) and granule size distribution (GSD), becomes one of the challenges in designing a dry granulation process. Therefore, an effective approach to predict ribbon solid fraction and GSD is essential to optimally operate the roller compactor.

Model-based approaches are commonly employed for design space analysis in pharmaceutical process and product development. Models can generally be categorized into three types: mechanistic models (or white-box models), data-driven models (or black-box models), and

* Corresponding author.
E-mail address: huan1289@purdue.edu (Y.-S. Huang).

https://doi.org/10.1016/j.compchemeng.2024.108586
Received 22 September 2023; Received in revised form 21 December 2023; Accepted 9 January 2024
Available online 10 January 2024

Nomenclature

A_{RF}	roller force calibration coefficient [kN/bar]
D_R	roller diameter [mm]
F	force factor [-]
K	compressibility factor [-]
$\dot{M}$	mass throughput [kg/h]
N_R	roller speed [rpm]
P_H	roller pressure [bar]
P_{max}	peak pressure [MPa]
S	roller gap [mm]
W	roller width [mm]
α	nip angle [rad] [°]
β	relaxation factor [-]
γ_0	pre-consolidation solid fraction [-]
γ_G	ribbon solid fraction at the roller gap [-]
γ_R	ribbon solid fraction [-]
δ_E	effective angle of internal friction [rad] [°]
ρ_t	true density [g/cm^3]
ϕ_W	wall friction angle [rad] [°]
θ	angular roll position [rad] [°]
σ	normal stress [MPa]
Q_v	cumulative bimodal Weibull distribution
a_1	weighting of the small mode [-]
p_1	size parameters of the small mode [μm]
p_2	size parameters of the large mode [μm]
m_1	shape parameters of the small mode [-]
m_2	shape parameters of the large mode [-]
N_{Mill}	mill speed [rpm]
S_{Lower}	lower screen size [mm]
S_{Upper}	upper screen size [mm]
S_M	rotor-screen gap [mm]
W_y, $W_{\Delta u}$	weighting matrices
u	input variables
Δu	control movements
$\hat{x}$	estimates state variables
y	output variables
$\hat{y}$	estimated output variables
y_{sp}	setpoints of the output variables
N_c	length of the control time window [-]
N_p	length of the prediction time window [-]
N_{past}	length of the past time window [-]
$\hat{\sigma}_\theta$	standard deviations of estimated model parameters
cov_θ	parameter covariance matrix
dof	degree of freedom [-]
RSS	residual sum of squares
H	Hessian approximation

hybrid models (or grey-box models). Firstly, mechanistic models are based on fundamental understanding of the underlying mechanisms in a system, and they typically incorporate relevant physical, chemical, and biological principles. While these models possess good interpretability, they may suffer from high computational expenses and plant-model mismatch when describing a real process. Secondly, data-driven models are developed purely from empirical data and generally consist of statistically based relationships. When the underlying system is not well understood or is too complex to be expressed by explicit equations, data-driven models are preferred for their adaptability in accurately predicting the system and easy development. However, the main challenges for data-driven models lie in poor generalizability and interpretability and the requirement of a large amount of data. Thirdly, mechanistic models and data-driven models can be integrated to form a hybrid model. This integration allows for incorporating the advantages of mechanistic and data-driven models while mitigating their respective drawbacks.

Mechanistic models such as Johanson's model (Johanson, 1965) and Reynolds' model (Reynolds et al., 2010) are typically used to describe roll compaction and predict the ribbon solid fraction produced. However, most ribbons can only be sampled and characterized once they exit the roll gap. Due to elastic recovery, the increased ribbon volume reduces the ribbon density. Elastic recovery is a common phenomenon in the field of powder compaction (e.g., roll compaction, tableting), and it can continue for several hours or days after compaction in some materials (Keizer and Kleinebudde, 2020; Picker, 2001). In addition, (Mahmah et al., 2019) indicated that the variation in the elastic recovery is a critical factor in ribbon splitting, which may cause adverse effects on the mechanical strength and dissolution properties of the tablets formed from the milled granules. While elastic recovery leads to uncertainty in roll compaction process and unsatisfactory prediction accuracy of ribbon solid fraction, it is either not considered or assumed to be a constant in the models reported in the literature.

In the ribbon milling step, the final GSD is determined by ribbon properties (e.g., ribbon density or porosity) and milling conditions (e.g., milling type, milling speed, and screen size). The GSD can sometimes be bimodal (Loreti et al., 2017; Mangal et al., 2016; Olaleye et al., 2020), making its prediction more challenging. A population balance model (PBM) can be used to describe the milling step and to predict GSD (Amini et al., 2020; Mirtič and Reynolds, 2016; Olaleye et al., 2019), but it is complicated to determine the breakage function in the PBM purely based on ribbon fracture physics. In addition, it is generally challenging to choose appropriate particle size intervals that balance the computational efficiency of solving the partial differential equations with model accuracy. Given the complex three-step nature of the ribbon milling process (ribbon crushing followed by upper and lower hammer milling), machine learning (ML) is a preferred alternative to developing a mechanistic model. For example, (Kazemi et al., 2016) demonstrated that GSD in the oscillating milling process can be accurately predicted by a genetic programming (GP) model or a neural network (NN) model. Moreover, ML and mechanistic model components can be combined into a hybrid model to maintain high physical interpretability and feasibility. For instance, (Akkisetty et al., 2010) developed a hybrid model to predict GSD in conical milling by using a neural network model to find the breakage function and selective function in PBM. However, the reported ribbon milling models lack adequate consideration of roll compaction parameters and ribbon properties. For the purpose of designing and controlling a continuous dry granulation process, both roll compaction models and ribbon milling models need to be integrated.

An integrated model is required not only for product design but also for real-time process monitoring and control. While open-loop control is still widely applied in the pharmaceutical industry, product quality can be compromised because of process disturbances and variability in raw materials properties. Advanced process control (APC) strategies can be employed to correct deviations in product qualities or process behavior as these occur. Model predictive control (MPC) is a common type of APC strategy, which can accommodate process constraints and complex processes involving multiple process inputs and outputs. To achieve continuous manufacturing and real-time release testing, MPC has progressed from "nice-to-have" to "must-have" technology in the pharmaceutical industry (J. Huang et al., 2021). While MPC has been widely applied in the processing industries (Lee, 2011; Lin et al., 2022; Qin and Badgwell, 2003), its use is still in the infant stage in the pharmaceutical manufacturing sector (Jelsch et al., 2021). Case studies of linear MPC implementation have been reported for powder feeding-blending system (Celikovic et al., 2020; Singh et al., 2014), the rotary tablet press (Su

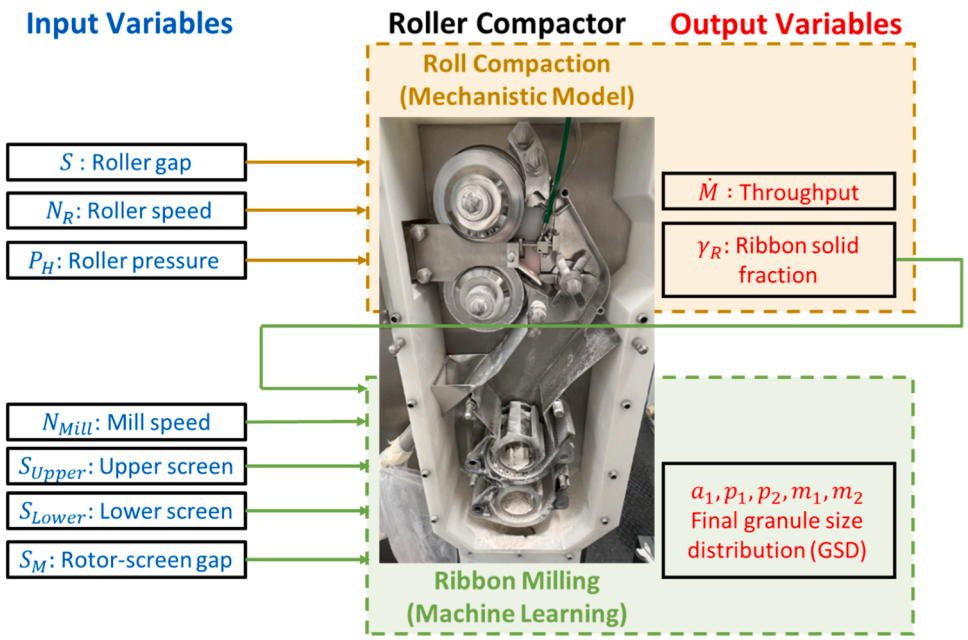

Fig. 1. Overview of the roller compactor model.

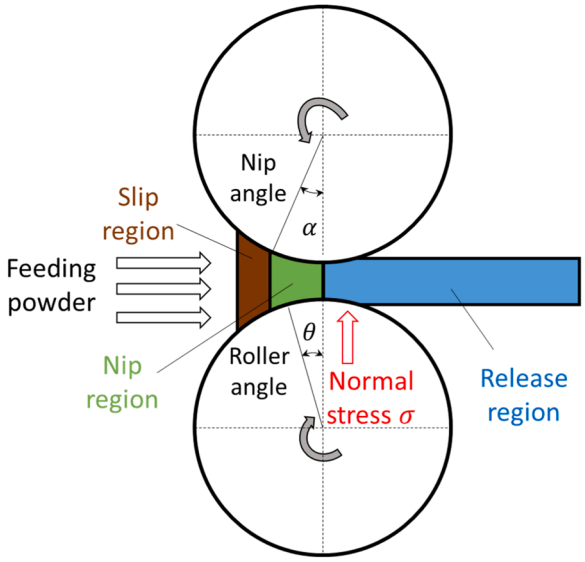

Fig. 2. Schematic diagram of the roll compaction process.

et al., 2019), and end-to-end continuous manufacturing pilot plant from chemical synthesis to tableting (Mesbah et al., 2017). Furthermore, nonlinear model predictive control (NMPC) has been applied to control a commercial-scale rotary tablet press in silico (Y. S. Huang et al., 2021) as well as demonstrated in a physical pilot plant (Huang et al., 2022b) and has been shown to achieve satisfactory control performance even when plant-model mismatch exists. However, MPC implementation in dry granulation processes has been limited. Singh and co-workers proposed a process control strategy based on cascade PID control in the dry granulation process. They indicated that MPC can be used to improve performance when oscillatory responses are observed (Singh et al., 2012).To the authors' knowledge, only one case study of MPC implementation in a roller compactor has been published (Hsu et al., 2010a). However, this study focused solely on controlling ribbon density and roll gap without incorporating throughput and GSD in the process control design.

The remainder of this article is structured as follows. The next section introduces a hybrid roller compactor model which integrates the roll compaction and ribbon milling processes and serves to predict RSF, throughput, and GSD. The third section presents the formulation of the NMPC problem and the process control system design. The fourth section summarizes the specifics of the case studies reported in this study. The results of model validation and NMPC implementation are presented in the fifth section. The final section summarizes the achievements of this paper and provides some future directions.

2. Roller compactor modeling

The roller compactor is the key unit operation of the continuous dry granulation process. The process input and output variables of the roller compactor are summarized in Fig. 1.

2.1. Roll compaction

According to Johanson's model (Johanson, 1965), the regions containing compacted materials can be divided into the slip region, where the rollers move faster than the powder in the slip region, and the nip region, where there is no slip between the roller and the powder as shown in Fig. 2. The stress gradient in the slip region and nip region can be expressed as follows:

$$\left(\frac{d\sigma}{d\theta}\right)_{slip} = \frac{4\sigma\left(\frac{\pi}{2}-\theta-\nu\right)\tan\delta_E}{\left(1+\frac{S}{D_R}-cos\theta\right)\left[\cot(A-\mu)-\cot(A+\mu)\right]} \tag{1}$$

$$\left(\frac{d\sigma}{d\theta}\right)_{nip} = \frac{K\sigma\left(2cos\theta-1-\frac{S}{D_R}\right)tan\theta}{\left(1+\frac{S}{D_R}-cos\theta\right)cos\theta} \tag{2}$$

where

$$A = \frac{\theta+\nu+\frac{\pi}{2}}{2} \tag{3}$$

$$\nu = \frac{1}{2}\left[\pi-\sin^{-1}\left(\frac{sin\phi_w}{sin\delta_E}\right)-\phi_W\right] \tag{4}$$

$$\mu = \frac{\pi}{4} - \frac{\delta_E}{2} \tag{5}$$

As the powder blend transitions from the slip condition to the non-slip condition, the stress gradients in the slip region and nip region become equal. The critical angular roller position at which this occurs is known as the nip angle α and can be calculated from Eqs. (1) and (2) and solving Eq. (6):

$$\frac{4\left(\frac{\pi}{2} - \alpha - \nu\right)\tan\delta_E}{\cot(A-\mu) - \cot(A+\mu)} - \frac{K\left(2cos\alpha - 1 - \frac{S}{D_R}\right)tan\alpha}{cos\alpha} = 0 \tag{6}$$

where δ_E is the effective angle of internal friction and ϕ_W is wall friction angle, K is compressibility factor, S is roller gap, and D_R is roller diameter. Given the roller diameter D_R and roller width W, the peak pressure P_{max} applied on the powders at the minimum roller gap S is computed as follows:

$$P_{max} = \frac{2P_H A_{RF}}{WD_R F} \tag{7}$$

with the force factor F, given by

$$F = \int_0^{\alpha} \left[\frac{\frac{S}{D_R}}{\left(1 - \frac{S}{D_R} - cos\theta\right)cos\theta} \right]^K cos\theta \, d\theta \tag{8}$$

where P_H is the roller pressure (or hydraulic pressure) and A_{RF} is the roll force calibration coefficient. Assuming that compression follows a power law, the ribbon solid fraction at the gap γ_G can be computed as follows:

$$\gamma_G = \gamma_0 (P_{max})^{\frac{1}{K}} \tag{9}$$

where $\gamma_0$is the pre-consolidation solid fraction and the peak pressure has to be divided by 1 MPa for a dimensionless value. However, γ_G is not readily measured in real time because the ribbon elastic relaxation causes the ribbon density to decrease over some time period when ribbons are released from the rollers. Given the relaxation factor β, the ribbon solid faction $\gamma_R$is represented as follows:

$$\gamma_R = \frac{\gamma_G}{\beta} \tag{10}$$

Considering mass balance around the roller gap and roller speed N_R, the mass throughput can be calculated as follows:

$$\dot{M} = \pi D_R W \left(S + S_{Comp}\right) N_R \rho_t \gamma_G = \pi D_R W \left(S + S_{Comp}\right) N_R \rho_t \beta \gamma_R \tag{11}$$

where ρ_t is the powder true density. In this work, a compensation term S_{Comp} is proposed to correct the volume of the powders that are bounded by rollers in cases when the roller surface is not smooth. When knurled rollers are used, it is necessary to take into account the volumes of powders which fill up the voids of the roller surface. The lower roller gap makes the powders in the voids occupy a higher percentage. It should be noted that elastic recovery and mass throughput calculations are not part of the original Johanson's model, described by Eqs. (1-8).

2.2. Ribbon milling

The hammer milling step commonly produces granules with a bimodal size distribution, which is not adequately described by only using D_{10}, D_{50} and D_{90} values. Therefore, a bimodal Weibull distribution is chosen to represent the entire size distribution where its cumulative form $Q_v(x)$ can be expressed as follows:

$$Q_v(x) = a_1 \left(1 - e^{-\left(\frac{x}{p_1}\right)^{m_1}}\right) + (1 - a_1)\left(1 - e^{-\left(\frac{x}{p_2}\right)^{m_2}}\right) \tag{12}$$

with constraints $0 \le a_1 \le 1$, $0 < p_1 < p_2$, and $1 < m_1, m_2$. Here, a_1 is the weighting of the smaller particle size portion, p_1 and p_2 are the size parameters of the smaller portion (or called the fines mode) and the larger portion (called coarse mode), respectively, whereas $m_1$and m_2 represent the shape parameters of the associated modes.

A neural network model is employed in this study to predict granule size distribution. For the nonlinear activation function domain, linear scaling with the range from 0.1 to 0.9 are applied to both input and output variables as follows:

$$\overline{z} = \frac{0.9 - 0.1}{z_{max} - z_{min}}(z - z_{min}) + 0.1 \tag{13}$$

where z and $\overline{z}$ are the raw and scaled values of process variables. The NN model with three layers (input, hidden, and output layers) and hyperbolic tangent activation function is given by:

$$\overline{Y} = L_2(\tanh(L_1\overline{U}) + C_1) + C_2 \tag{14}$$

where $L_1 \in \mathbb{R}^{n_N \times n_U}$, $L_2 \in \mathbb{R}^{n_Y \times n_N}$, $C_1 \in \mathbb{R}^{n_N \times 1}$ and $C_2 \in \mathbb{R}^{n_Y \times 1}$ are fitting model parameters. The NN model output Y is composed of five fitting parameters of the bimodal Weibull distribution: $Y = [a_1, p_1, p_2, m_1, m_2]^T$. The NN model inputs U include upper screen size, lower screen size, mill speed, rotor-screen gap, and ribbon solid fraction: $U = [S_{Upper}, S_{Lower}, N_{Mill}, S_M, \gamma_R]^T$.

3. Process control design

3.1. NMPC formulation

The PID control strategy, while well-established and extensively applied in various industries for several decades, has some limitations. These limitations stem from the fact that PID controllers are inherently designed for linear single-input-single-output (SISO) systems. While PID controllers can deliver satisfactory control performance in nonlinear systems, provided that the operation region is linear or mildly nonlinear, the control performance can deteriorate in multiple-input-multiple-output (MIMO) systems. In such systems, strong process interactions can make tuning PID controllers challenging. In addition, PID controllers rely on current measurements, and gross errors in sensor measurements can thus compromise their control performance. These limitations of PID controllers have spurred the interest in the development and adoption of more advanced process control strategies to manage complexities inherent in MIMO systems. The MPC algorithm utilizes a finite time horizon over which to optimize the control inputs starting at the current time interval. It outperforms typical PID control because MIMO systems and process constraints can be easily handled within the MPC optimization framework. Future process events can be anticipated with the aid of process models, but such predictions do impose requirements on model accuracy.

Linear MPC has been widely implemented in several industries because it is relatively easy to develop linear models using data-driven system identification techniques or linearization of nonlinear models. The models commonly used are linear state space models, whose general form facilitates quick prediction of process dynamics. Moreover, the standardized form of linear state space models allows for applying a generalized and systematic approach to assess critical aspects such as stability, controllability, and robustness during the design of control strategies (Dubljevic and Humaloja, 2020; Qin and Badgwell, 1997). However, the control performance over a larger range of operations obtained by linear models can degrade if the system is highly nonlinear. Additionally, the physical interpretability of the parameters within a

linear state space model could be compromised. By contrast, NMPC obtained by using a high-fidelity nonlinear model can accurately describe process trajectories but at the expense of higher computation cost. Due to the lack of a standardized form in the nonlinear model utilized in NMPC formulation, assessing stability or robustness becomes more challenging compared to linear MPC. The decision to implement linear MPC or NMPC should be based on a balance among computational expense, accuracy requirements, and the degree of system nonlinearity.

Processes that take place in the continuous pharmaceutical manufacturing systems are known to be nonlinear in nature. In the oral solid dosage manufacturing processes, nonlinearity is evident across various stages, such as organic synthesis (Mesbah et al., 2017), crystallization (Orehek et al., 2021), filtration-washing-drying process (Destro et al., 2021; Hur et al., 2024), feeding and blending (Liu et al., 2018; Rehrl et al., 2016), dry granulation (Hsu et al., 2010b; Singh et al., 2012; Souihi et al., 2015), tableting (Bachawala and Gonzalez, 2022; Galbraith et al., 2019; Y. S. Huang et al., 2021; Singh et al., 2013), and film coating (Mesbah et al., 2014). The nonlinear behavior observed in these processes can be attributed to several factors, including complex chemical reactions, heat and mass transfer, powder flowability, and powder compression mechanisms.

Hsu et al.'s work (Hsu et al., 2010a) demonstrated that NMPC can outperform both linear MPC and PID control in simulated studies, particularly in terms of disturbance rejection and setpoint tracking for controlling ribbon solid fraction. This study will focus on the experimental implementation of NMPC and explore the extension of this control strategy to ribbon milling processes.

The discrete formulation of the NMPC optimization problem at time $t = k$ can be described as:

$$\min_{\Delta u_t} J = \sum_{t=k}^{k+N_p} \left(\hat{y}_t - y_{sp}\right)^T W_y \left(\hat{y}_t - y_{sp}\right) + \sum_{t=k}^{k+N_c-1} \left(\Delta u_t^T W_{\Delta u} \Delta u_t\right) \tag{15a}$$

subject to

$$\hat{x}_{k+j+1} = f\left(\hat{x}_{k+j}, \hat{u}_{k+j}, \theta\right) \tag{15b}$$

$$\hat{y}_{k+j} = h\left(\hat{x}_{k+j}\right) + \zeta_k \tag{15c}$$

$$\Delta u_{k+j} = \hat{u}_{k+j+1} - \hat{u}_{k+j} \tag{15d}$$

$$\hat{x}_{k+j} \in \mathbb{X},\ \hat{u}_{k+j} \in \mathbb{U},\ \Delta u_{k+j} \in \Omega_{\Delta u} \tag{15e}$$

$$j = 0,\ 1,\ \ldots,\ N_p - 1 \tag{15f}$$

where $\hat{x}_t$ are the estimates of the state variables at time t. The variable $\hat{y}_t$ represents the estimated output variables and y_{sp} are the setpoints of the output variables. Control movements Δu are constrained to lie in a compact set $\Omega_{\Delta u}$. W_y and $W_{\Delta u}$ are the weighting matrices. N_c and N_p are the length of the control time window and prediction time horizon, respectively. The control window N_c is usually smaller than the prediction window N_p and has to be chosen to compromise between the computational time and control stability requirements. Control movements Δu_{k+j} in control window N_c vary according to results of optimization, but those beyond the control window are zero, i.e., $\Delta u_{k+N_c} = \Delta u_{k+N_c+1} = \cdots = \Delta u_{k+N_p-1} = 0$, which implies that $\hat{u}_{k+N_c} = \hat{u}_{k+N_c+1} = \cdots = \hat{u}_{k+N_p}$. In other words, while the predicted $\hat{y}_{k+j}$ can still be calculated using Δu_{k+j} and $\hat{u}_{k+j}$ in the prediction window N_p, only Δu_{k+j} in control window N_c is considered in the objective function. For the purpose of zero steady-state offset in controlled output variables y, output disturbances ζ_k at time $t = k$ in Eq. (15c) can be represented as follows:

$$\zeta_k = median\left\{y_{k-N_{past}+j} - \hat{y}_{k-N_{past}+j}\right\},\ \text{for } j = 0,\ 1,\ \ldots,\ N_{past} \tag{16}$$

where N_{past} is the length of the past time window. It should be noted that

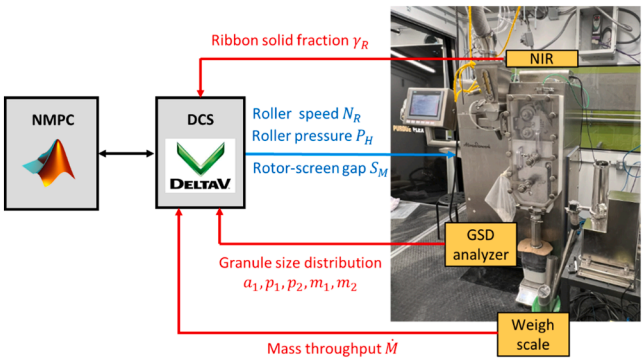

Fig. 3. Process control structure for the roller compactor.

while an error distribution of output variables $y_t - \hat{y}_t$ in the past time window can be obtained, a single point estimate of the output is of most interest in many applications (Rao et al., 2003). In this study, the median of the error distribution in the past time window is used to represent output disturbances.

3.2. NMPC implementation

The process control structure employed in this study is illustrated in Fig. 3. The NMPC framework is implemented using MATLAB, and the optimization problem in each iteration is solved using MATLAB's built-in *fmincon* function which employs an interior point algorithm. This local optimization solver function can't guarantee a global optimum, but it can quickly ensure a reliable and satisfactory local solution at each time interval. The Emerson DeltaV 13.3 distributed control system (DCS) is utilized to integrate measurements from the roller compactor and the PAT tools. The DCS's OPC server acts as a bridge to collect process data from the roller compactor and PAT tools, as well as to transmit control commands to the roller compactor (Chen et al., 2023). The performance of NMPC is evaluated through two case studies: (1) focusing solely on the roll compaction process with two inputs and two outputs, discussed in Section 5.3, and (2) examining the integrated roll compaction and ribbon milling process with three inputs and seven outputs, detailed in Section 5.4. A summary of the corresponding process variables and control design can be found in Table 1.

Table 1
Summary of variables and details of NMPC implementation in the two case studies.

	Roll compaction	Roll compaction + Ribbon milling
Section	5.3	5.4
Implementation	Experiments	Simulation
Manipulated variables (u)	Roller speed N_R Roller pressure P_H	Roller speed N_R Roller pressure P_H Rotor-screen gap S_M
Controlled variables (y)	Mass throughput $\dot{M}$ Ribbon solid fraction γ_R	Mass throughput $\dot{M}$ Ribbon solid fraction γ_R Granule size distribution a_1, p_1, p_2, m_1, m_2
Hardware	Intel®Xeon® CPU E3–1246 v3 @3.50GHz 8GB RAM	Intel® Core ™ i7–11800H @ 2.30GHz 16GB RAM
MATLAB version	2015b	2021b
Time window length $[N_p, N_c, N_{past}]$	[30,10,30]	[30,10,30]
Sampling time (s)	2	2
Computation time (s)	1.4	1.3

Table 2
Properties of the feeding material (blend of MCC-102 and APAP) and the roller compactor.

Properties	Value
True density (ρ_t)	1.5583 g/cm^3
D_{10}	146.8 μm
D_{50}	301.6 μm
D_{90}	492.5 μm
Wall friction angle (ϕ_W)	35.1°
Effective angle of internal friction (δ_E)	44.5°
Roller diameter (D_R)	120 mm
Roller width (W)	40 mm
Roll force calibration coefficient (A_{RF})	0.369 kN/bar

4. Materials and methods

4.1. Materials and equipment

Acetaminophen Grade 0048 (APAP) was purchased from Mallinckrodt Pharmaceuticals (Raleigh, NC, USA). Avicel microcrystalline cellulose Grade PH-102 (MCC-102) was purchased from IMCD US, LLC (Piscataway, NJ, USA). The formulation used in this study is 10 wt% APAP and 90 wt% MCC-102. To prepare feeding materials for the roller compactor, a 3 kg blend of APAP and MCC-102 was mixed using a 5 L Tote blender for 30 min.

The study utilizes an Alexanderwerk WP 120 roller compactor, which is depicted in Fig. 3 and further detailed in Fig. 1. The equipment is operated with knurled rollers with dimensions of 40 mm in width and 120 mm in diameter. The unit employs a two-stage hammer mill

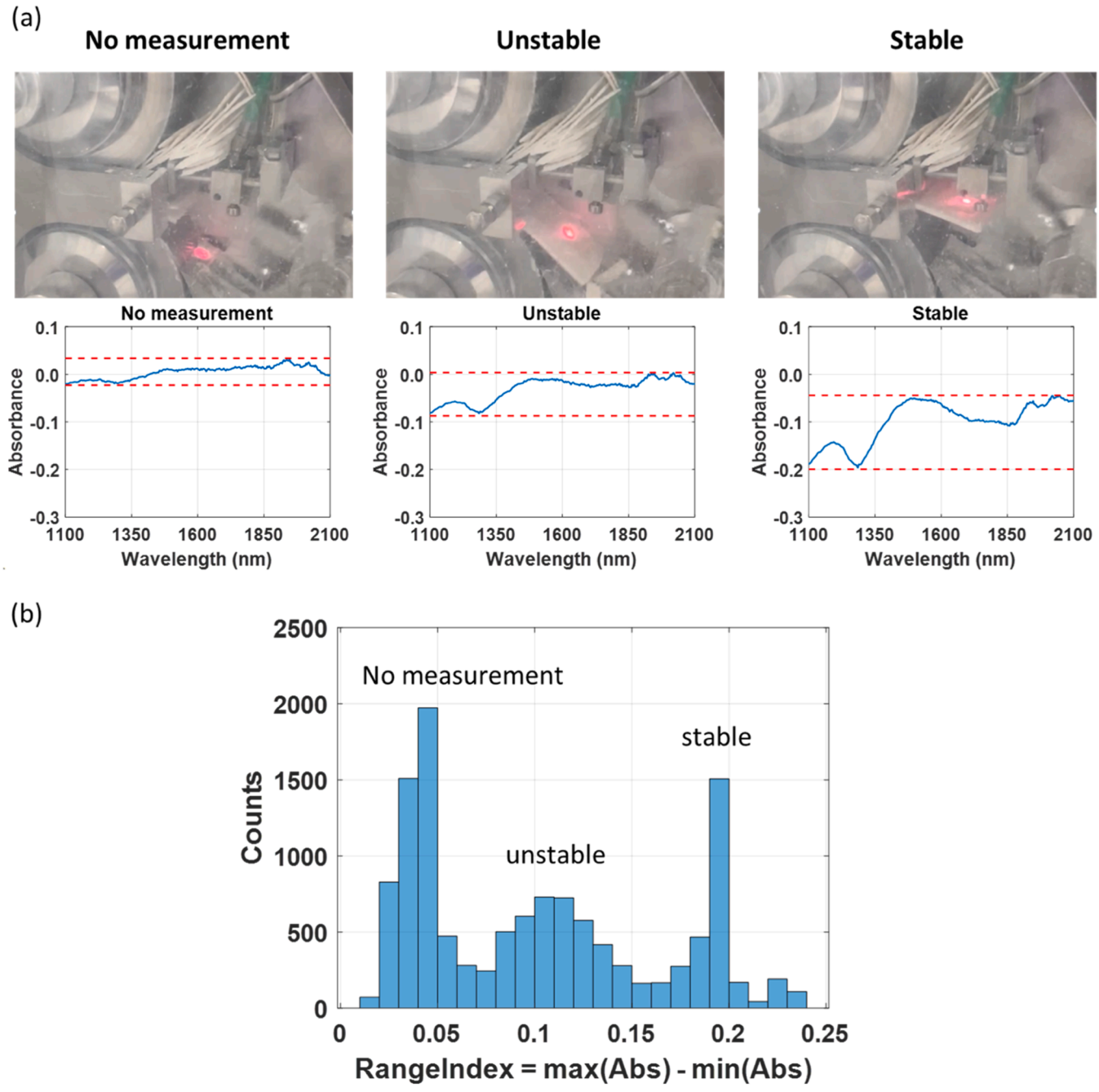

Fig. 4. Real-time monitoring of ribbon solid fraction with (a) raw spectra and (b) range index under different conditions.

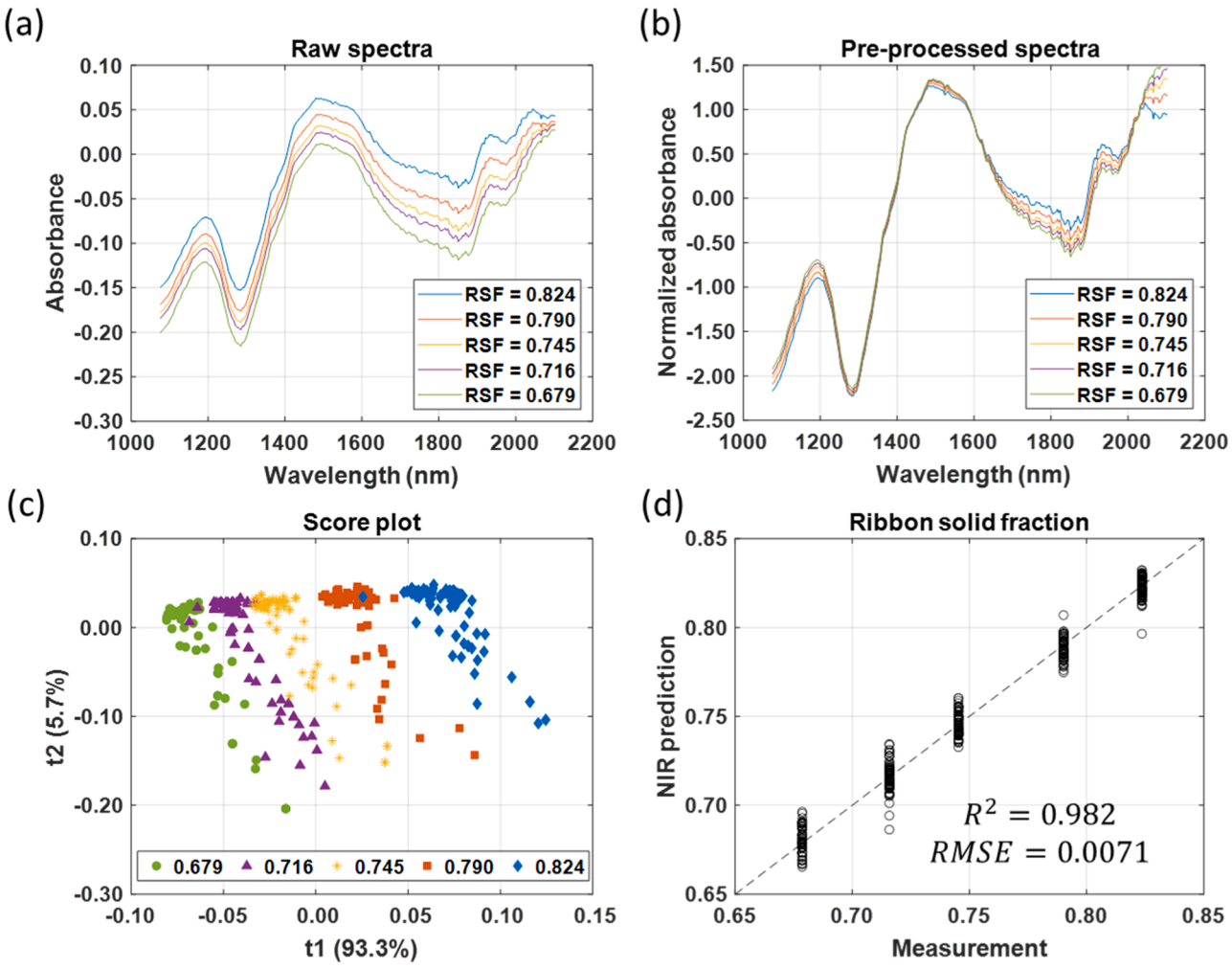

Fig. 5. Performance of NIR calibration model to predict real-time ribbon solid fraction (RSF) with (a) raw spectra, (b) pre-processed spectra, (c) score plot and (d) parity plot.

equipped with two distinct screen sizes: an upper screen for pre-milling and a lower screen for final milling. Screens are installed on rotating cams, which can adjust the gap between the rotors and screens. Although different rotor-screen gaps can be set for the pre-mill and final mill, this study simplifies the process by assigning the same setpoints to both mills.

The properties of the feeding material and the WP 120 roller compactor are summarized in Table 2. The wall friction angle and the effective angle of internal friction are estimated based on the work by (Mahmah et al., 2019).

4.2. Product characterization and experimental procedure

Three key instruments were utilized to validate the roller compactor model to obtain the desired process outputs. Firstly, as an in-house real-time flow rate sensor, a Mettler Toledo ME 4001E weighing scale was positioned at the exit of the roller compactor. The weighing scale was connected to a laptop via a RS232 cable, enabling the recording of the total weight of accumulated granules using the MATLAB Instrument Control Toolbox. By calculating the first-order derivative with respect to time, the real-time flow rate can be determined. Secondly, the Geopyc 1360 pycnometer was employed to measure the ribbon envelop density (ρ_e). The ribbon solid fraction (γ_R) can be calculated as follows:

$$\gamma_R = \frac{\rho_e}{\rho_t} \tag{17}$$

where ρ_t is the powder true density, which is measured by an Accupyc II 1340 pycnometer. Thirdly, the final GSD was measured using the SolidSizer, manufactured by J.M. Canty Inc. Over 40 different types of size and shape characteristics can be captured with the SolidSizer. In this study, the projected area of each particle was chosen as a key characteristic which was converted to the circular equivalent diameter to represent the size of the feed powder blend and granules. It should be noted that the cumulative frequency of the GSD was volume-based in this study. Once the size percentiles (D_5, D_{10}, …, D_{95}) are obtained through statistical analysis, the bimodal Weibull distribution parameters can be computed by solving an optimization problem (Huang et al., 2023):

$$\min_{a,\ p_1,\ p_2, m_1, m_2} J = \sum_{p=5,10,\ldots}^{95} \left(\frac{i}{100} - Q_v(D_p) \right)^2 \tag{18}$$

$$\textit{subject to } 0 \le a \le 1,\ 0 < p_1 < p_2,\ 1 < m_1,\ m_2$$

To evaluate the performance of the milling models, the mean absolute percentage error (MAPE) of GSD is utilized and can be computed as follows:

$$MAPE = \sum_{i=1}^{n} \sum_{p=5,10,\ldots}^{95} \left| \frac{D_{p,i}^{pred} - D_{p,i}}{D_{p,i}} \right| \times 100\% \tag{19}$$

In conducting the experiments, a K-Tron QT20 loss-in-weight (LIW)

Table 3
Experimental values of process inputs and outputs in the roll compaction process.

Exp	Process inputs			Process outputs		Ribbon status	Role in model
	Roller gap S [mm]	Roller speed N_R [rpm]	Roller pressure P_H [bar]	Ribbon solid fraction γ_R	Mass throughput $\dot{M}$ [kg/h]		
C1	1.20	4.0	44.9	0.761	6.35	Non-split	Test
C2	1.20	4.0	73.9	0.816	7.45	Non-split	Training
C3	1.36	4.0	30.5	0.660	6.53	Non-split	Test
C4	1.40	4.0	36.9	0.696	7.39	Non-split	Training
C5	1.40	4.0	58.9	0.743	7.57	Non-split	Training
C6	1.40	4.0	74.1	0.812	7.97	Non-split	Test
C7	1.60	4.0	30.6	0.681	7.67	Non-split	Training
C8	1.60	4.0	37.0	0.684	7.81	Split	Training
C9	1.80	4.0	30.6	0.640	7.67	Non-split	Training
C10	1.80	6.0	28.6	0.601	12.60	Non-split	Training
C11	1.80	8.0	28.7	0.632	15.41	Non-split	Training
C12	1.80	4.0	44.8	0.745	8.55	Split	Training
C13	1.80	6.0	44.6	0.664	11.25	Split	Test
C14	1.80	8.0	44.9	0.717	16.66	Split	Training
C15	2.00	4.0	30.6	0.648	9.17	Non-split	Training
C16	2.00	4.0	44.6	0.699	10.06	Split	Training
C17	2.20	4.0	30.6	0.648	9.80	Split	Training
C18	2.40	4.0	28.6	0.617	10.01	Split	Training

feeder was utilized to feed pre-blended materials into the roller compactor continuously. The roller compactor was operated for approximately three minutes to reach a steady state. Subsequently, an additional three minutes of operation was dedicated to estimating the average mass throughput. Finally, samples of the ribbons and granules were collected from the roller compactor for measurements of ribbon solid fraction and GSD.

4.3. Model parameter estimation

To estimate the parameters of the roll compaction model, the MATLAB *fmincon* function with interior point algorithm was used to minimize the error in the predicted mass throughput and ribbon solid fraction. To increase the likelihood of finding a global solution, the MATLAB *GlobalSearch* algorithm was used, under which the *fmincon* function is repeatedly executed from multiple starting points. Instead of employing several iterations in linear regression of Eq. (9) in logarithm form to determine pre-consolidation solid fraction γ_0 and compressibility factor K, a combined optimization problem is formulated as follows to estimate model parameters:

$$\min_{K,\ \gamma_0,\ \beta,\ S_{Comp}} J = \sum_{i=1}^{n} \left[\left(\frac{\gamma_{R,i} - \gamma_{R,i}^{pred}}{\gamma_{R,i}} \right)^2 + \left(\frac{\dot{M}_i - \dot{M}_i^{pred}}{\dot{M}_i} \right)^2 \right] \tag{20}$$

For the ribbon milling model, the training of the neural network model was conducted using PyTorch, a Python-based machine learning library, in Python 3.9 (Paszke et al., 2019). The objective was to minimize the mean squared error in the five fitted Weibull parameters. To construct the NN model, *torch.nn.Sequential, torch.nn.Linear*, and *torch.nn.Tanh* were utilized. The weighting and constants for each neuron of the NN model (i.e., L_1, L_2, C_1, C_2 in Eq. (14)) were trained using the Adam optimizer (Kingma and Ba, 2014). The 5-fold cross-validation method was applied to prevent overfitting. Three neurons were used in the hidden layer. To develop the NN model, 23 datasets were designated for training and 6 datasets were used for testing, according to the 80/20 rule.

4.4. NIR calibration for real-time measurements of ribbon solid fraction

The Geopyc 1360 pycnometer is effective for measuring ribbon solid fraction but is limited to off-line analysis. For real-time measurement of ribbon solid fraction, the Innopharma Multieye2 NIR spectrometer was utilized with the fiber optic probe positioned on the platform above the ribbon. The NIR light wavelength ranges from 1076 nm to 2102 nm, and the integration time was set to 180 ms. In Fig. 4(a), three kinds of spectra were observed during the operation of the roller compactor. When the ribbon emerged and was detected by the NIR probe, stable spectra were obtained as long as the distance between the probe and the ribbon remained constant. However, when the ribbon came into contact with the flake crusher, variations in the distance between the NIR probe and the ribbon caused unstable spectra measurement. Finally, when the ribbon was completely broken and no material was detected, the NIR spectra displayed only the characteristics of the metal. To differentiate between these three types of spectra quantitatively, a range index was introduced, defined by the difference between the maximum and minimum absorbance values. The range index of all the collected spectra exhibits a tri-modal distribution in Fig. 4(b), supporting the observance of three types of spectra. Only range indexes larger than the threshold value of 0.15 were considered to ensure that only stable spectra were utilized for calibration model development. This choice balances model reliability and sampling time, as setting the threshold too high would increase sampling time.

Five ribbon solid fractions, ranging from 0.679 to 0.824, were selected to calibrate the NIR model. Around 70 spectra were collected for each ribbon solid faction. Fig. 5 summarizes the steps and analysis of the calibration model. The averaged absorbance values of the raw spectra for each ribbon solid fraction are depicted in Fig. 5(a), revealing a clear trend of increasing absorbance with higher ribbon solid fractions. To eliminate the negative impact of baseline shifts, the raw spectra were normalized using the standard normal variate (SNV) method, where each spectrum is subtracted by its mean and then divided by its standard deviation. The normalized spectra were then employed to train a partial least squares (PLS) regression model. Three principal components were selected, and the first two components, t1 and t2, accounted for 99 % of the total variance (93.3 % and 5.7 %, respectively), as shown in Fig. 5(c). The resulting NIR calibration model demonstrated excellent performance, as evidenced by the high R^2 value of 0.982 and low RMSE value of 0.0071. This NIR model will be used to obtain the real-time process control results reported in Section 5.3.

5. Results and discussion

5.1. Roll compaction model validation

For model development and validation, 80 % of the data was randomly selected for training, and the remaining 20 % was used for testing. In this work, two roll compaction models were validated and evaluated using 14 sets of training data and 4 sets of test data, as indicated in Table 3. All experiments were performed in gap-controlled

Table 4
Estimated roll compaction model parameters and associated model evaluation.

	Traditional model	Proposed model with compensated roll gap
K	4.189 ± 0.412	4.828 ± 0.624
γ_0	0.307 ± 0.027	0.291 ± 0.025
β	1.244 ± 0.021	1.051 ± 0.091
S_{Comp} [mm]	0	0.318 ± 0.175
$RMSPE(\gamma_R)$(training) [%]	2.86	2.77
$RMSPE(\gamma_R)$ (test) [%]	3.47	3.51
$RMSPE(\dot{M})$ (training) [%]	4.44	3.87
$RMSPE(\dot{M})$ (test) [%]	9.59	9.17
$R^2(\gamma_R)$ (training)	0.88	0.89
$R^2(\gamma_R)$ (test)	0.87	0.86
$R^2(\dot{M})$ (training)	0.97	0.98
$R^2(\dot{M})$ (test)	0.70	0.74

mode, where the roller compactor automatically adjusted the feed screw speed to maintain the desired roller gap, roller speed, and roller pressure. The operating region was determined to run the roller compactor at low throughput, encompassing low roller gap, roller speed, and roller pressure. The rationale for this was to extend the duration of the experiment, providing a demonstration of the NMPC implementation with the consumption of less input material. The setpoints for the roller gap were established at [1.2, 1.4, 1.6, 1.8, 2.0, 2.2, 2.4] mm, while the roller speed and roller pressure were set at [4, 6, 8] rpm and [30, 37, 45, 60, 75] bar, respectively. The values in Table 3 are real measurements, which slightly deviate from setpoints. A design of experiments was employed to investigate the effects of varying operational process parameters. Specifically, the impact of the roller gap was assessed through datasets [C3, C7, C9, C15, C17, C18] and [C1, C12, C16]; the influence of roller speed was examined via datasets [C9, C10, C11] and [C12, C13, C14]; and the effect of roller pressure was explored through datasets [C1, C2], [C3, C4, C5, C6], [C7, C8], and [C15, C16].

The estimated model parameters and their respective model performance for both the traditional model and the proposed model are summarized in Table 4. The traditional model estimated the mass throughput without considering the surface texture of the rollers (smooth or knurled). It assumed that the roller gap's compensation term S_{Comp} in Eq. (11) was zero, as previously reported in some literature (Reynolds et al., 2010; Toson et al., 2019). On the other hand, the proposed model in this study incorporated this consideration if knurled rollers are used. Based on the evaluation metrics of root mean squared percentage error (RMSPE) and R^2 values, the proposed model demonstrates similar prediction accuracy for the ribbon solid fraction and slightly better prediction accuracy for the mass throughput than the traditional model. To assess the model identifiability, the standard deviations of the estimated model parameters are presented in Table 4. These standard deviations can be computed as follows (Casas-Orozco et al., 2021):

$$\hat{\sigma}_\theta = \sqrt{diag(cov\ _\theta)} \tag{21}$$

with the parameter covariance matrix $cov\ _\theta$, given by

$$cov\ _\theta = \frac{RSS}{dof} H^{-1} \tag{22}$$

where the degree of freedom (dof) is equal to the difference between the number of training data sets and the number of estimated parameters. RSS is the residual sum of squares and H is the Hessian approximation. In Table 4, the standard deviations of the model parameters in the proposed model are higher than those in the traditional model, suggesting higher level of uncertainty in the proposed model. This higher uncertainty can be attributed to estimating one more parameter in the proposed model when the same amount of training data is used.

Considering the physical implications when knurled rollers are used, the proposed model offers better alignment with reality and avoids violating the constraint that the ribbon solid fraction (γ_G and γ_R) should be less than 1. The relaxation factor (β) may not be crucial when focusing solely on predicting the ribbon solid fraction (γ_R) because it can be lumped with pre-consolidation ribbon solid fraction (γ_0) to become $\frac{\gamma_0}{\beta}$, however, it becomes significant for continuous manufacturing scenarios where accurate mass throughput prediction is essential for achieving state of control. The values of the relaxation factor obtained can be significantly different depending on the approach used. It can be determined based on the (1) ratio of ribbon thickness to roller gap, (2) the ratio of mass flow rate to ribbon density, or (3) by solving an optimization problem as done in this study. The use of knurled rollers makes it challenging to accurately measure the ribbon thickness and roller gap. Consequently, a modification was made to the mass throughput model to account for the volumes of voids between the embossments on the knurled rollers. Although these voids are small, they can constitute a substantial percentage, especially when the roll gap is low.

When using the traditional model to achieve good predictions for both the ribbon solid fraction (γ_R) and mass throughput, it may be necessary to overestimate the ribbon solid fraction at the gap (γ_G) by lowering K and increasing $\gamma_0$to compensate for the model's disregard of the underestimated volume between two knurled rollers. Although increasing the relaxation factor (β) in the traditional model can improve the prediction accuracy for the ribbon solid fraction, it risks violating the physical meaning because the ribbon solid fraction should not exceed 1. For instance, if β is equal to 1.244, the ribbon solid fraction (γ_R) cannot exceed 1/1.244 = 0.804, but Exp C2 and C6 in Table 3 show the

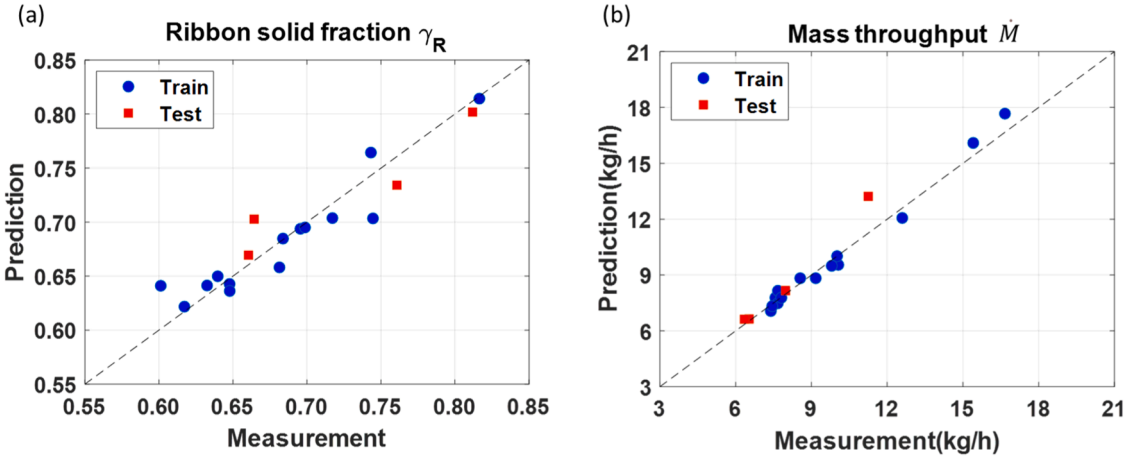

Fig. 6. Performance of proposed roll compaction model to predict (a) ribbon solid fraction and (b) mass throughput.

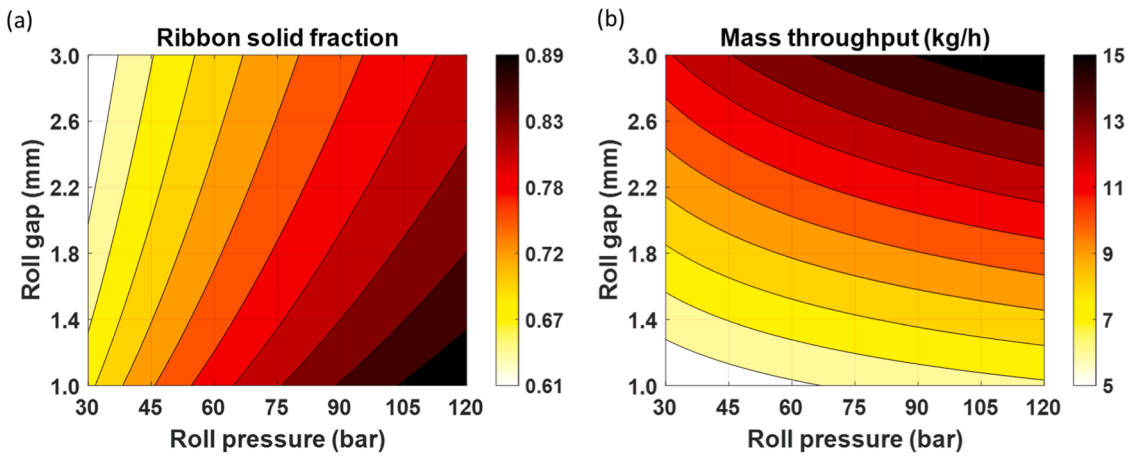

Fig. 7. Design space for (a) ribbon solid fraction and (b) mass throughput based on the proposed roll compaction model.

Table 5
Experimental values of process inputs and outputs in the ribbon milling process.

Exp	Process inputs					Process outputs					Fitting MAPE [%]
	Upper screen [μm]	Lower screen [μm]	Mill speed [rpm]	Rotor screen gap [mm]	Predicted ribbon solid fraction	a_1	p_1 [μm]	p_2 [μm]	m_1	m_2	
M1	2500	800	25	1.0	0.694	0.892	592	714	2.24	11.95	0.7
M2	2500	800	25	1.0	0.802	0.840	596	677	2.12	7.11	0.7
M3	2500	800	100	1.0	0.802	0.850	604	604	2.85	1.48	2.0
M4	2500	1250	25	1.0	0.636	0.400	410	1013	2.52	3.10	0.6
M5	2500	1250	25	1.0	0.643	0.488	385	1027	2.62	3.50	0.9
M6	2500	1250	25	1.0	0.644	0.432	395	1025	2.59	3.25	0.7
M7	2500	1250	60	0.5	0.664	0.194	404	919	2.74	4.20	0.3
M8	2500	1250	60	1.0	0.665	0.305	468	978	2.66	4.06	0.4
M9	2500	1250	60	1.5	0.664	0.285	440	999	2.75	4.39	0.6
M10	2500	1250	25	1.0	0.658	0.488	432	1074	2.54	4.15	0.8
M11	2500	1250	25	1.0	0.703	0.328	460	1177	2.41	4.72	0.9
M12	2500	1250	25	1.0	0.736	0.380	360	1036	2.73	2.75	1.2
M13	3150	1250	25	1.0	0.764	0.237	408	1073	2.27	3.81	0.5
M14	3150	1250	100	1.0	0.764	0.245	432	996	2.28	4.22	0.4
M15	2000	1250	25	1.0	0.764	0.310	459	1143	2.30	4.40	0.4
M16	2000	1250	100	1.0	0.765	0.286	508	1181	2.18	4.86	0.3
M17	2500	1250	60	0.5	0.768	0.182	455	1095	2.14	4.32	0.7
M18	2500	1250	60	1.0	0.768	0.247	417	1126	2.30	4.38	1.9
M19	2500	1250	60	1.5	0.768	0.302	482	1106	2.22	4.82	0.5
M20	2500	1250	25	1.0	0.804	0.347	363	1103	2.58	3.31	1.1
M21	2500	1600	25	1.0	0.662	0.292	461	1390	2.22	4.36	0.8
M22	2500	1600	60	1.0	0.663	0.171	435	1496	2.28	3.64	1.0
M23	2500	1600	25	1.0	0.693	0.474	803	1502	1.98	5.85	0.7
M24	2500	1600	100	1.0	0.693	0.301	550	1445	2.07	4.10	0.9
M25	2500	1600	60	1.0	0.733	0.484	947	1560	1.89	5.76	0.6
M26	2500	1600	25	1.0	0.777	0.220	605	1527	2.04	4.45	1.0
M27	2500	1600	60	1.0	0.777	0.250	665	1506	1.99	4.80	1.5
M28	2500	1600	25	1.0	0.802	0.330	933	1532	1.76	4.72	0.7
M29	2500	1600	100	1.0	0.802	0.154	497	1382	2.33	4.45	0.8

violation in the traditional model. Therefore, the proposed model provides a more realistic representation, ensuring accurate predictions without compromising the physical constraints of the system.

The proposed model exhibited satisfactory prediction accuracy within the range of ribbon solid fraction [0.60, 0.82] and mass throughput [6.4, 16.7] kg/h, as shown in Fig. 6. Furthermore, the model can be used to explore the design space. Fig. 7(a) illustrates that higher roller pressure increases ribbon solid fraction and flow rate. On the other hand, a larger roller gap reduces ribbon solid fraction, but enhances mass throughput due to the inclusion of more materials, as depicted in Fig. 7(b), where the roller speed is 4 rpm.

5.2. Ribbon milling model validation

In this work, ribbon milling models were validated and evaluated using the data shown in Table 5, including 23 sets of training data and 6 sets of test data (M7, M12, M16, M21, M22, M29). To develop a hybrid model, the ribbon solid fraction predicted from the roll compaction model is used as an input in the ribbon milling model. The measured GSD is assumed to follow the bi-modal Weibull distribution, which can be described by five parameters a_1, p_1, p_2, m_1, and m_2. These parameters can be easily used to obtain traditional percentile values such as D_{10}, D_{50}, and D_{90}. Two data-driven models were compared, namely, the multiple linear regression (MLR) model and the NN model. When predicting five bimodal Weibull parameters, the NN model shows a better accuracy, as shown in Fig. 8(a), particularly in predicting a_1, p_1, and m_2. Despite the NN model's ability to handle the nonlinearity in GSD prediction better than the MLR model, the high RMSPE values in predicting a_1, p_1, and m_2 indicate the challenges associated with their prediction. By contrast, the model can accurately predict p_2, which can be attributed

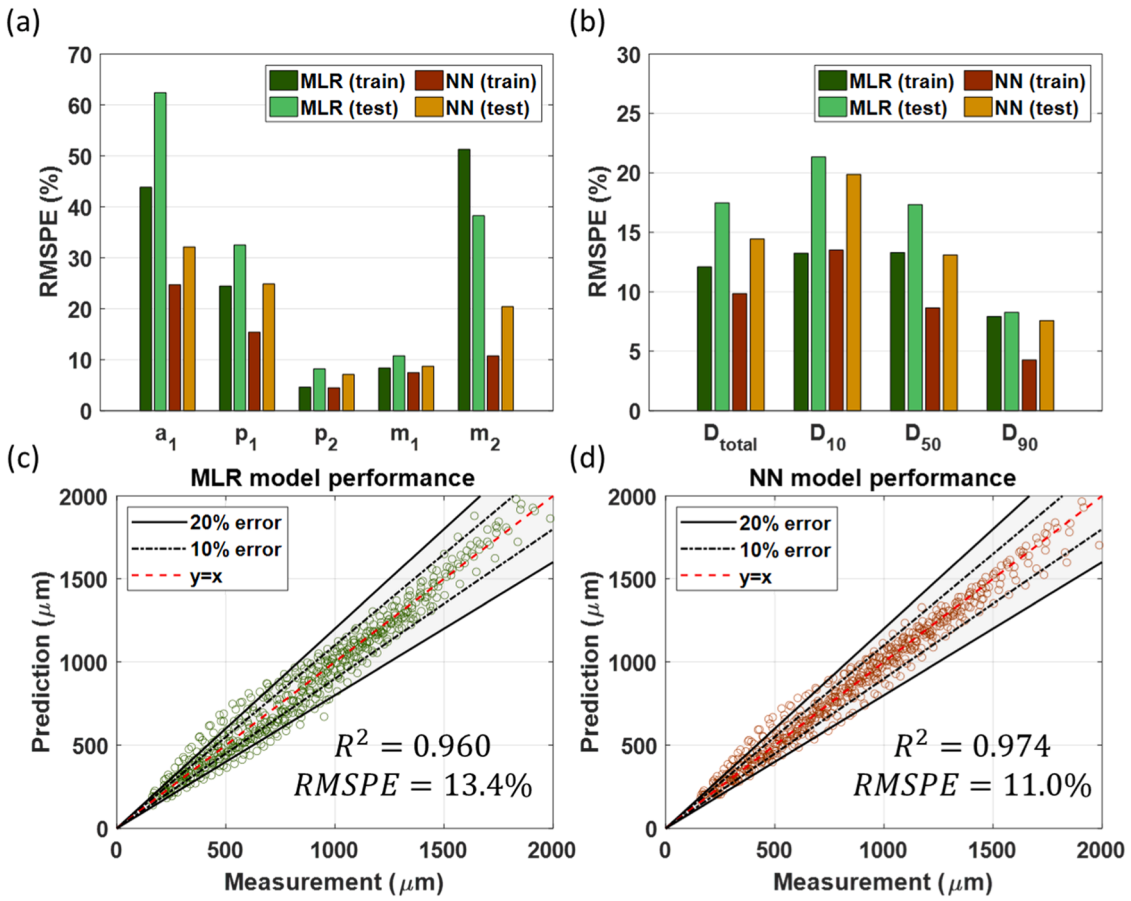

Fig. 8. Evaluations of ribbon milling models based on RMSPE of (a) five bimodal Weibull parameters and (b) percentiles of granule size as well as the parity plots based on (c) MLR and (d) NN models.

to the lower screen size determining the maximum size that can pass through the screen mesh.

By converting a_1, p_1, p_2, m_1, and m_2 to percentiles of granule size (D_5, D_{10}, …, D_{95}), the model performance can be also evaluated based on the RMSPE of size, as depicted in Fig. 8(b). The NN model outperforms the MLR model by exhibiting lower RMSPE of D_{total} based on all the percentiles ranging from D_5, D_{10}, … to D_{95}. In addition, it is observed that predicting low percentiles is more challenging than predicting high percentiles, as evidenced by the highest RMSPE in D_{10} and the lowest RMSPE in D_{90}. This might be attributed to the uncertainty in powder fines generation. Furthermore, predictions of all the percentiles ranging from D_5, D_{10}, … to D_{95} based on the MLR and NN models are displayed in Fig. 8(c) and Fig. 8(d), respectively. The accuracy of predicting size gradually improved from the smaller size to the larger size, again suggesting that the model is better at predicting higher percentiles. Overall, the NN model achieves an RMSPE of 11.0 % in predicting the entire size distribution.

The ribbon milling model offers valuable insights for product design and process control by predicting the entire GSD. Previous studies have highlighted the significance of the entire GSD in predicting the flowabilities of granules produced through wet granulation (Lagare et al., 2022) and dry granulation process (Lagare et al., 2023). In addition, the ratio of fines to coarse granules is crucial in determining granule bulk density and tabletability. Fig. 9 illustrates how the NN model can be employed to explore the influence of process inputs on the GSD. Lower screen size emerges as the most influential factor affecting the GSD, as demonstrated in Fig. 9(a). Granules passing through smaller lower screen sizes tend to exhibit unimodal GSD, while larger screen sizes make the bimodal nature of GSD more obvious. Fig. 9(b) reveals that an increase in ribbon solid fraction leads to increased granule size and a reduced percentage of fines. While larger granules are desirable for improved flowability, excessive compaction of the ribbon should be prevented since it can compromise tabletability. One of the novel aspects of this study is incorporating the rotor screen gap into the model to predict the GSD. However, it should be noted that manipulation of the rotor screen gap might not be available for all roller compactors. As shown in Fig. 9(c), reducing the rotor screen gap decreases the percentage of fines. This can be attributed to the larger rotor screen gap preventing the material from being fully pushed through the screen within a single milling cycle. Fig. 9(d) illustrates that an increase in the upper screen size can lead to a decrease in granule size. This phenomenon may be attributed to the fact that larger intermediate granules have a higher likelihood of being further milled when passing through the lower screen. Finally, Fig. 9(e) demonstrates that an increase in mill speed can reduce the size of the granules. This reduction in size is likely due to the granules being crushed more times at higher mill speeds.

In this study, an APAP-based formulation is used due to APAP being a commonly used API model compound in the literature. Its well-understood properties have been extensively studied. Additionally, APAP is relatively inexpensive, enabling us to run multiple experiments during the initial stages of developing new models or methods. This study is focused on demonstrating a model that links process parameters with GSD and ribbon solid fraction. For the ultimate objective of predicting granule flowability and tabletability in other formulations, these steps might be considered in the future work: (1) Identifying critical material properties, such as powder flowability, powder density, and powder compressibility. (2) Developing a model that utilizes material properties and process parameters to predict GSD and ribbon solid fraction. (3) Establishing a model that incorporates material properties, GSD, and ribbon solid fraction to predict granule flowability and

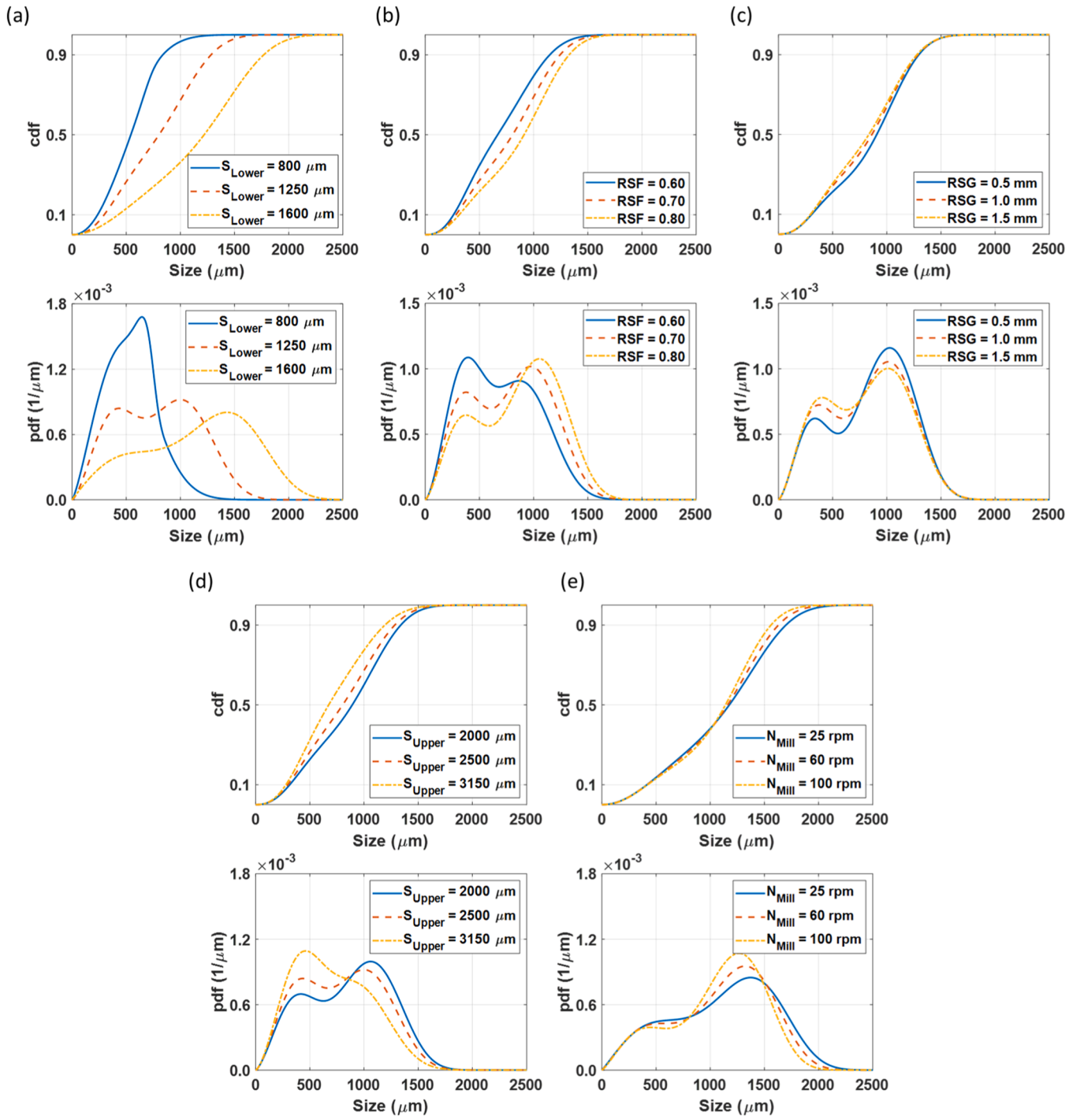

Fig. 9. Granule size distribution in the ribbon milling process under the impact of (a) lower screen size, (b) ribbon solid fraction, (c) rotor screen gap, (d) upper screen size, and (e) mill speed.

tabletability.

5.3. NMPC on roll compaction process (experiments)

An open-loop experiment was conducted to evaluate the performance of the roll compaction model and real-time sensors, and the corresponding time series data are presented in Fig. 10. The first manipulated variable, roller speed, was fixed at 4 rpm, as shown in Fig. 10(b). Three step changes were introduced to the second manipulated variable, roller pressure, as shown in Fig. 10(c). Due to operating the roller compactor in gap-controlled mode, the feed-screw speed was automatically increased to feed more materials whenever roller pressure was enhanced, as shown in Fig. 10(a). To prevent ribbon splitting, which could potentially damage the NIR probe, a roll gap of 1.4 mm was maintained throughout the experiment, as shown in Fig. 10(d). The experimental results in Section 5.1 indicate that ribbon splitting can be avoided by lowering the roll gap and roll pressure. It is also observed that undershooting in the roll gap happens whenever the roll pressure setpoint increases because the local PLC controller in the roller compactor prioritizes reaching the roll pressure setpoint.

Fig. 10(e) illustrates the first process output variable, mass throughput. Both the model and measurements capture the increasing

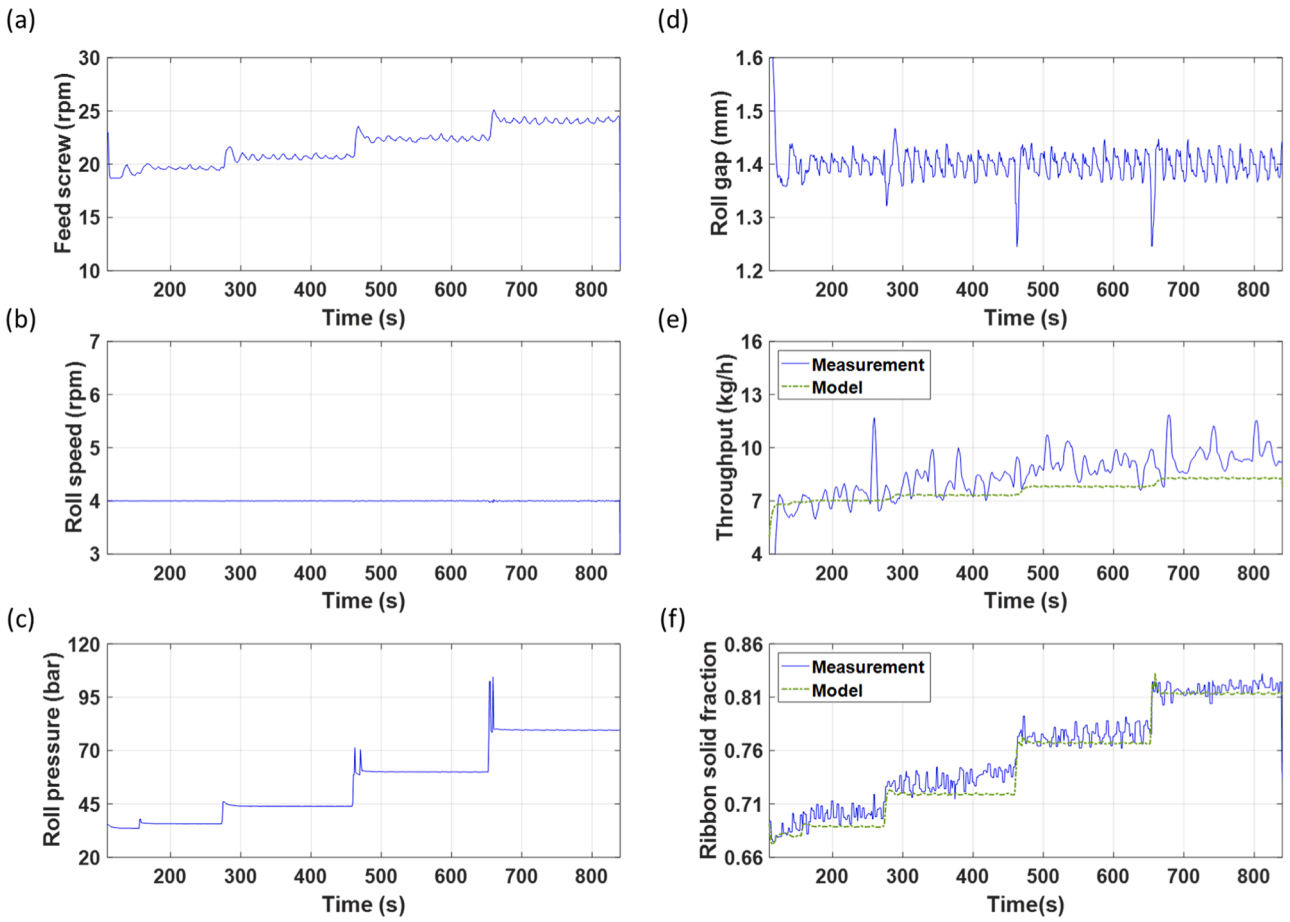

Fig. 10. Open loop control of roll compaction process.

trend as the roll pressure is raised. Examining four time intervals (t1 = 160 ~240 s, t2 = 310~450 s, t3 = 480~640 s, and t4 = 670~830 s), the model exhibits RMSPE values of 7.5 %, 12.3 %, 14.7 %, and 15.0 % respectively. The model tends to underestimate the granule flow rate more significantly over time. This underestimation can be attributed to two possible reasons: (1) the model's construction in Section 5.1 did not allow enough time for the flow rate to reach an actual steady state during experiments, and (2) sampling of ribbons and granules led to a lower measured flow rate. Additionally, spikes in the flow rate were observed due to the sudden drop of fines accumulated in the chamber. Regarding the second process output variable, ribbon solid fraction, as shown in Fig. 10(f), the model demonstrates excellent accuracy with an RMSPE of 1.6 % for time t = 160 to 830 s. These satisfactory model predictions and real-time process measurements provide a strong foundation for NMPC implementation.

Fig. 11 illustrates the implementation of a 2-by-2 NMPC for the roll compaction process. The granule flow rate was maintained at 10 kg/h, as shown in Fig. 11(e), while the ribbon solid fraction was set to 0.73, 0.81, and 0.77, as shown in Fig. 11(f). Offsets were notably observed when the control loop remained open before time t = 120 s. However, once NMPC was initiated, it exhibited remarkable setpoint tracking capabilities. The NMPC efficiently determined the optimal roller pressure in response to new setpoints for the ribbon solid fraction. To maintain a consistent flow rate, the roller speed was automatically adjusted in the opposite direction to compensate for ribbon solid fraction changes, particularly evident at time t = 300 s and t = 480 s. Given the inherent disturbances in the roll compaction process arising from fines accumulation and the discontinuity of ribbon production, the NMPC demonstrated effective disturbance rejection abilities. In addition, it is important to note that since NMPC actively adjusts process inputs, it also resulted in increased variation in the roll gap. Fig. 11(d) shows that the standard deviation of the roller gap increased from 0.012 mm (during time t = 50 ~ 100 s) to 0.034 mm (during time t = 180 ~650 s). To quantify the control performance of open-loop control and NMPC, Table 6 displays the integral absolute error (IAE) values for mass throughput and ribbon solid fraction. The evaluation of the open-loop control is based on the time window from t = 20~120 s, while that of NMPC is conducted over the period t = 200~300 s in Fig. 11. The lower IAE values observed for NMPC indicate its superior capability in setpoint tracking and disturbance rejection compared to open-loop control.

5.4. NMPC of integrated dry granulation process (simulation)

In addition to controlling ribbon solid fraction and mass throughput described in the previous section, GSD should be controlled in real time to ensure the product qualities in the dry granulation process. The results of an in-silico NMPC implementation of a dry granulation process, including roll compaction and ribbon milling, are illustrated in Fig. 12. Specifically, Fig. 12 (a-c) represents the process behavior of three process inputs: roller speed, roller pressure, and rotor-screen gap. Fig. 12 (d-j) demonstrates the corresponding seven process outputs: mass throughput, ribbon solid fraction, and GSD parameters (a_1, p_1, p_2, m_1, and m_2). Such non-square control systems where the numbers of process inputs and outputs are different provide another motivation for using the NMPC framework.

There are three critical takeaways from Fig. 12. First, when the control loop is open before time t = 200 s, noticeable offsets are observed in all the process outputs. However, once NMPC is initiated, it rapidly reaches all the setpoints for the process outputs. Secondly, at time t = 400 s, the setpoint for the ribbon solid fraction is increased from

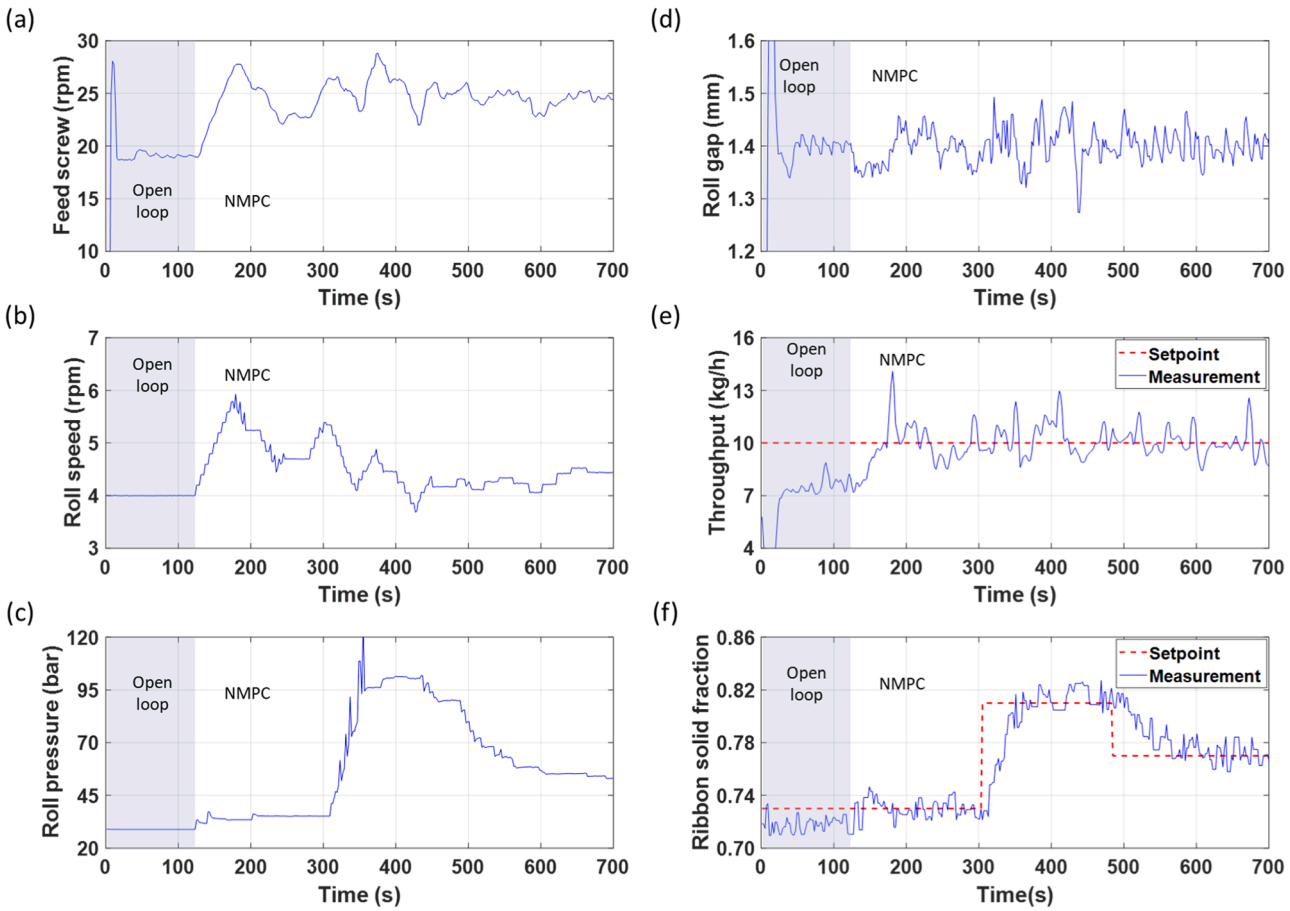

Fig. 11. NMPC experimental implementation on roll compaction process.

Table 6
Comparison of control performance between open-loop control and NMPC in the roll compaction process.

	Open-loop control	NMPC
IAE (Throughput) [s kg/h]	269.92	78.68
IAE (Ribbon solid fraction) [s]	1.22	0.54

0.7 to 0.8. This increase in ribbon solid fraction can disturb the GSD, leading to a reduction in fines (e.g., decreasing a_1) and an increase in particle size (e.g., increasing p_1 and p_2). With the aid of NMPC, the controller identifies the necessary adjustment of the rotor-screen gap to compensate for this effect. By increasing rotor-screen gap, more fines can be produced to enable the GSD to remain closer to the setpoint. It is important to note that a non-square control system has its limitations, as offsets may occur if the setpoints are not within the feasible design space. In this instance, the change in ribbon solid fraction was deliberately increased. Nonetheless, in reality, disturbances in ribbon solid fraction can often arise due to factors such as variability in powder density and roller gap. Even in such cases, the actuator of the rotor-screen gap can effectively mitigate its impact on GSD, showing the robust disturbance rejection capability in this process control strategy. Thirdly, at time = 1200s, a setpoint change is introduced to the GSD, shifting the values from $[a_1, p_1, p_2, m_1, m_2] = [0.29, 411, 1050, 2.49, 3.96]$ to [0.22, 368, 1066, 2.49, 4.20]. Since this new targeted GSD falls within the feasible region, the controller can determine the optimal rotor screen gap required to achieve it. Subsequently, another step change for GSD is introduced at time = 1600s, adjusting the values to $[a_1, p_1, p_2, m_1, m_2] = [0.37, 432, 985, 2.54, 3.64]$, and the ribbon solid fraction is increased from 0.7 to 0.63. The NMPC successfully finds the optimal values for all three process inputs in each scenario, demonstrating its satisfactory capability for setpoint tracking.

To move forward with the NMPC implementation in the physical dry granulation process controlling GSD, several challenges must be addressed. Firstly, the availability of real-time GSD measurements is essential. Although attempts have been made to install a camera-based system in the pilot plant, the occurrence of powder fouling hinders measurement robustness. Despite the utilization of an air purging system, the fouling still compromises the accuracy of the measurement. To overcome this challenge, one possible solution is to incorporate at-line measurements, such as the Canty Solidizer, and implement an automated granule sampling approach to obtain GSD measurements. In addition, remote control of the rotor screen gap via the DCS is necessary. For the roller compactor used in this study, the rotor screen gap can only be adjusted through the local control panel's human-machine interface. By allowing remote control via the DCS, the NMPC framework could fully control the entire GSD.

6. Conclusions

The hybrid model effectively predicts three critical outputs in the dry granulation process: ribbon solid fraction, mass throughput, and GSD. This model integrates a mechanistic roll compaction model with a neural network-based ribbon milling model. The assessment of the hybrid model reveals that incorporating a roll gap compensation term not only aids in estimating a realistic ribbon relaxation factor but also enhances the model's accuracy in predicting ribbon solid fraction and mass throughput. Furthermore, the model employs five bimodal Weibull distribution parameters to comprehensively describe the entire GSD, reducing the complexity of model output variables and providing a clear

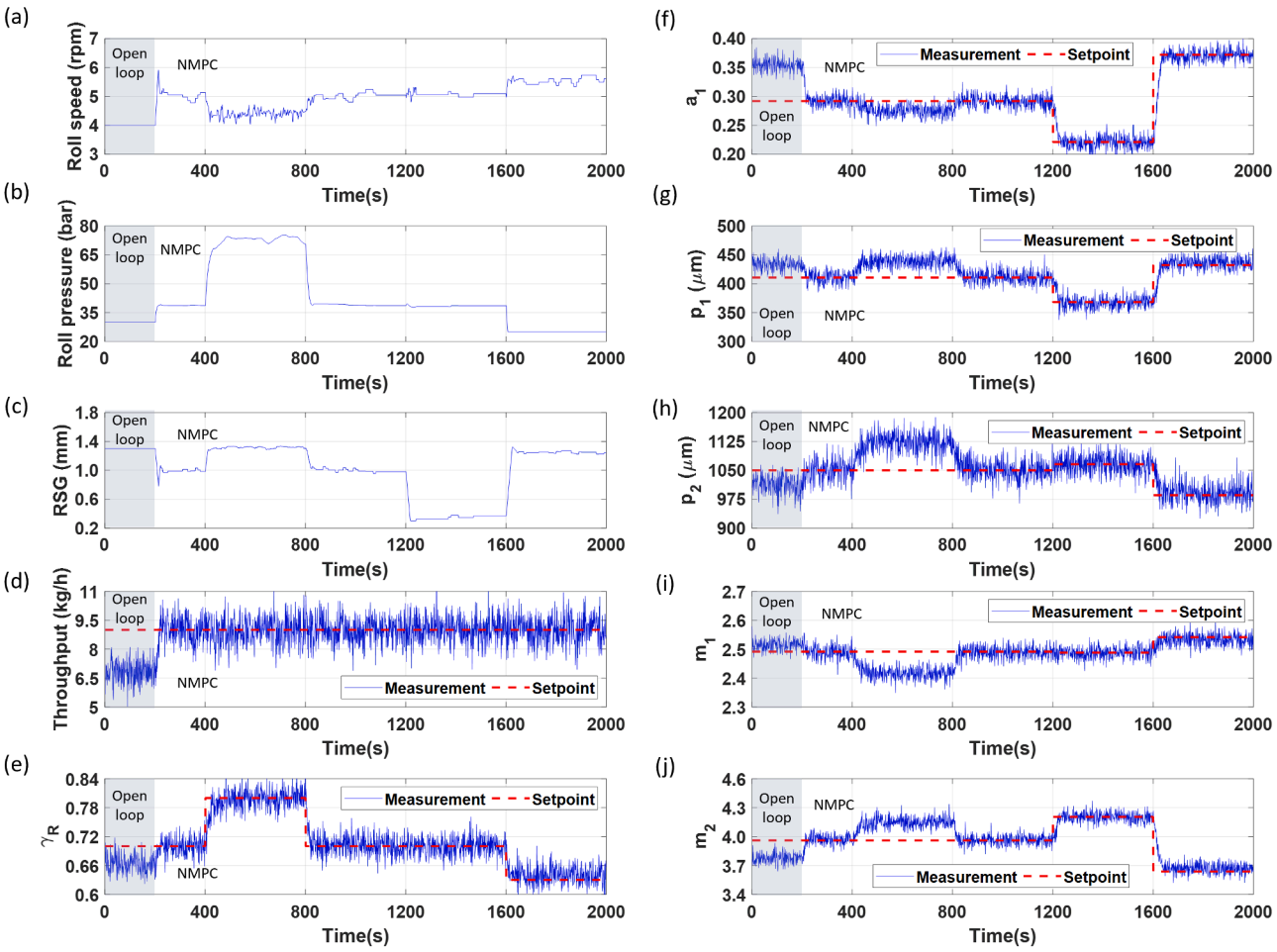

Fig. 12. NMPC performance of integrated dry granulation process including three process inputs (a-c) and seven process outputs (d-j).

understanding of how process parameters influence GSD. Reducing the proportion of fines can be achieved by increasing the lower screen size and ribbon solid fraction or decreasing the rotor screen gap. Utilizing the proposed hybrid model, NMPC was successfully implemented to control the dry granulation process effectively. The efficacy of NMPC was demonstrated in two case studies. The first experimental case study validated NMPC's ability to control mass flow rate and ribbon solid fraction, provided by the proposed NIR analysis approach to select stable spectra. Moreover, in the second simulated case study, NMPC demonstrated its ability to handle the entire GSD, rather than relying on a representative size value like the median size. This simulated case study showed how NMPC can handle a non-square system, again providing the motivation to use NMPC instead of traditional open-loop control.

In future work, it is essential to incorporate constraints when improving the ribbon milling model. The current limitation of the neural network model is that if the operating conditions deviate significantly from the training data set, the predicted GSD may violate the limitations imposed by the bimodal Weibull distribution. In addition, efforts should be made to enhance the accuracy in predicting smaller size percentiles because the percentage of fines can impact tabletability. Furthermore, additional modeling work is required to establish the relationship between granule properties and tablet properties. By integrating such a model, NMPC can be effectively implemented on an end-to-end dry granulation-based tableting line.

CRediT authorship contribution statement

Yan-Shu Huang: Conceptualization, Formal analysis, Investigation, Methodology, Software, Writing – original draft. **Rexonni B. Lagare:** Conceptualization, Formal analysis, Investigation. **Phoebe Bailey:** Conceptualization, Formal analysis, Investigation. **David Sixon:** Conceptualization, Formal analysis, Investigation. **Marcial Gonzalez:** Conceptualization, Funding acquisition, Supervision, Writing – review & editing. **Zoltan K. Nagy:** Conceptualization, Funding acquisition, Supervision, Writing – review & editing. **Gintaras V. Reklaitis:** Conceptualization, Funding acquisition, Supervision, Writing – review & editing.

Declaration of competing interest

The authors declare that they have no known competing financial interests or personal relationships that could have appeared to influence the work reported in this paper.

Data availability

Data will be made available on request.

Acknowledgements

This material is based upon work supported by the National Science Foundation under Grant No. 2140452 - CMMI-EPSRC: Right First Time Manufacture of Pharmaceuticals (RiFTMaP).

References

Akkisetty, P.K., Lee, U., Reklaitis, G.V., Venkatasubramanian, V., 2010. Population balance model-based hybrid neural network for a pharmaceutical milling process. J. Pharm. Innov. 5, 161–168. https://doi.org/10.1007/s12247-010-9090-2.

Amini, H., Palahnuk, H., Akseli, I., 2020. Population balance modeling (PBM) of ribbon milling in pharmaceutical roller compaction process. Powder Technol. 376, 438–457. https://doi.org/10.1016/j.powtec.2020.08.036.

Bachawala, S, Gonzalez, M, 2022. Development of mechanistic reduced order models (ROMs) for glidant and lubricant effects in continuous manufacturing of pharmaceutical solid-dosage forms. ESCAPE 51, 1129–1134. https://doi.org/10.1016/b978-0-323-95879-0.50189-2.

Casas-Orozco, D., Laky, D., Wang, V., Abdi, M., Feng, X., Wood, E., Laird, C., Reklaitis, G. V., Nagy, Z.K., 2021. PharmaPy: an object-oriented tool for the development of hybrid pharmaceutical flowsheets. Comput. Chem. Eng. 153 https://doi.org/10.1016/j.compchemeng.2021.107408.

Celikovic, S., Kirchengast, M., Rehrl, J., Kruisz, J., Sacher, S., Khinast, J., Horn, M., 2020. Model predictive control for continuous pharmaceutical feeding blending units. Chem. Eng. Res. Design 154, 101–114. https://doi.org/10.1016/j.cherd.2019.11.032.

Chen, Y., Sampat, C., Huang, Y.-S., Ganesh, S., Singh, R., Ramachandran, R., Reklaitis, G. V., Ierapetritou, M., 2023. An integrated data management and informatics framework for continuous drug product manufacturing processes: a case study on two pilot plants. Int. J. Pharm. 642, 123086. https://doi.org/10.1016/j.ijpharm.2023.123086.

Destro, F., Hur, I., Wang, V., Abdi, M., Feng, X., Wood, E., Coleman, S., Firth, P., Barton, A., Barolo, M., Nagy, Z.K., 2021. Mathematical modeling and digital design of an intensified filtration-washing-drying unit for pharmaceutical continuous manufacturing. Chem. Eng. Sci. 244, 116803 https://doi.org/10.1016/j.ces.2021.116803.

Dubljevic, S., Humaloja, J.P., 2020. Model predictive control for regular linear systems. Automatica 119. https://doi.org/10.1016/j.automatica.2020.109066.

Fonteyne, M., Vercruysse, J., De Leersnyder, F., Van Snick, B., Vervaet, C., Remon, J.P., De Beer, T., 2015. Process Analytical Technology for continuous manufacturing of solid-dosage forms. TrAC. https://doi.org/10.1016/j.trac.2015.01.011.

Galbraith, S.C., Cha, B., Huang, Z., Park, S., Liu, H., Meyer, R.F., Flamm, M.H., Hurley, S., Zhang-Plasket, F., Yoon, S., 2019. Integrated modeling of a continuous direct compression tablet manufacturing process: a production scale case study. Powder Technol. 354, 199–210. https://doi.org/10.1016/j.powtec.2019.05.078.

Herting, M.G., Kleinebudde, P., 2008. Studies on the reduction of tensile strength of tablets after roll compaction/dry granulation. Eur. J. Pharmaceutics Biopharmaceutics 70, 372–379. https://doi.org/10.1016/j.ejpb.2008.04.003.

Hsu, S.H., Reklaitis, G.V., Venkatasubramania, V., 2010a. Modeling and control of roller compaction for pharmaceutical manufacturing: part II: control system design. J. Pharm. Innov. 5, 24–36. https://doi.org/10.1007/s12247-010-9077-z.

Hsu, S.H., Reklaitis, G.V., Venkatasubramanian, V., 2010b. Modeling and control of roller compaction for pharmaceutical manufacturing. Part I: process dynamics and control framework. J. Pharm. Innov. 5, 14–23. https://doi.org/10.1007/s12247-010-9076-0.

Huang, J., O'Connor, T., Ahmed, K., Chatterjee, S., Garvin, C., Ghosh, K., Ierapetritou, M., Jeffers, M., Pla, D.L., Lee, S.L., Lovett, D., Lyngberg, O., Mack, J., McManus, E., Romero-Torres, S., Undey, C., Venkatasubramanian, V., Warman, M., 2021a. AIChE PD2M advanced process control workshop-moving APC forward in the pharmaceutical industry. J. Adv. Manuf. Process 3. https://doi.org/10.1002/amp2.10071.

Huang, Y.S., Sixon, D., Bailey, P., Lagare, R.B., Gonzalez, M., Nagy, Z.K., Reklaitis, G.V., 2023. A Machine Learning-assisted Hybrid Model to Predict Ribbon Solid Fraction, Granule Size Distribution and Throughput in a Dry Granulation Process. pp. 813–818. https://doi.org/10.1016/B978-0-443-15274-0.50130-X.

Huang, Y.S., Medina-González, S., Straiton, B., Keller, J., Marashdeh, Q., Gonzalez, M., Nagy, Z., Reklaitis, G.V., 2022a. Real-Time monitoring of powder mass flowrates for plant-wide control of a continuous direct compaction tablet manufacturing process. J. Pharm. Sci. 111, 69–81. https://doi.org/10.1016/j.xphs.2021.06.005.

Huang, Y.S., Sheriff, M.Z., Bachawala, S., Gonzalez, M., Nagy, Z.K., Reklaitis, G.V., 2021b. Evaluation of a combined mhe-nmpc approach to handle plant-model mismatch in a rotary tablet press. Processes 9. https://doi.org/10.3390/pr9091612.

Huang, Y.S., Sheriff, M.Z., Bachawala, S., Gonzalez, M., Nagy, Z.K., Reklaitis, G.V., 2022b. Application of MHE-based NMPC on a rotary tablet press under plant-model mismatch. Computer Aided Chemical Engineering. Elsevier B.V., pp. 2149–2154. https://doi.org/10.1016/B978-0-323-85159-6.50358-4

Hur, I., Casas-Orozco, D., Laky, D.J., Destro, F., Nagy, Z.K., 2024. Digital design of an integrated purification system for continuous pharmaceutical manufacturing. Chem. Eng. Sci. 285, 119534. https://doi.org/10.1016/j.ces.2023.119534.

Jelsch, M., Roggo, Y., Kleinebudde, P., Krumme, M., 2021. Model predictive control in pharmaceutical continuous manufacturing: a review from a user's perspective. Eur. J. Pharm. Biopharm. 159, 137–142. https://doi.org/10.1016/j.ejpb.2021.01.003.

Johanson, J.R., 1965. A rolling theory for granular solids. J. Appl. Mech. Trans. ASME 32, 842–848. https://doi.org/10.1115/1.3627325.

Kazemi, P., Khalid, M.H., Szlek, J., Mirtič, A., Reynolds, G.K., Jachowicz, R., Mendyk, A., 2016. Computational intelligence modeling of granule size distribution for oscillating milling. Powder Technol. 301, 1252–1258. https://doi.org/10.1016/j.powtec.2016.07.046.

Keizer, H.L., Kleinebudde, P., 2020. Elastic recovery in roll compaction simulation. Int. J. Pharm. 573 https://doi.org/10.1016/j.ijpharm.2019.118810.

Kingma, D.P., Ba, J., 2014. Adam: a method for stochastic optimization. In: Proceeding of the 3rd International Conference for Learning Representations.

Lagare, R.B., da Conceicao, M.A., Rosario, A.C.A., Young, K.L., Huang, Y.S., Sheriff, M.Z., Clementson, C., Mort, P., Nagy, Z., Reklaitis, G.V., 2022. Development of a Virtual Sensor for Real-Time Prediction of Granule Flow Properties. pp. 1081–1086. https://doi.org/10.1016/b978-0-323-95879-0.50181-8.

Lagare, R.B., Huang, Y.S., Bush, C.O.-J., Young, K.L., Rosario, A.C.A., Gonzalez, M., Mort, P., Nagy, Z.K., Reklaitis, G.V., 2023. Developing a virtual flowability sensor for monitoring a pharmaceutical dry granulation line. J. Pharm. Sci. https://doi.org/10.1016/j.xphs.2023.01.009.

Lee, J.H., 2011. Model predictive control: review of the three decades of development. Int. J. Control Autom. Syst. https://doi.org/10.1007/s12555-011-0300-6.

Lin, K.H., Eason, J.P., Biegler, L.T., 2022. Multistage nonlinear model predictive control for pumping treatment in hydraulic fracturing. AlChE J. 68 https://doi.org/10.1002/aic.17537.

Liu, J., Su, Q., Moreno, M., Laird, C., Nagy, Z., Reklaitis, G., 2018. Robust state estimation of feeding–blending systems in continuous pharmaceutical manufacturing. Chem. Eng. Res. Des. 134, 140–153. https://doi.org/10.1016/j.cherd.2018.03.017.

Loreti, S., Wu, C.Y., Reynolds, G., Mirtič, A., Seville, J., 2017. DEM–PBM modeling of impact dominated ribbon milling. AlChE J. 63, 3692–3705. https://doi.org/10.1002/aic.15721.

Mahmah, O., Adams, M.J., Omar, C.S., Gururajan, B., Salman, A.D., 2019. Roller compaction: ribbon splitting and sticking. Int. J. Pharm. 559, 156–172. https://doi.org/10.1016/j.ijpharm.2019.01.031.

Mangal, H., Kirsolak, M., Kleinebudde, P., 2016. Roll compaction/dry granulation: suitability of different binders. Int. J. Pharm. 503, 213–219. https://doi.org/10.1016/j.ijpharm.2016.03.015.

Mesbah, A., Ford Versypt, A.N., Zhu, X., Braatz, R.D., 2014. Nonlinear model-based control of thin-film drying for continuous pharmaceutical manufacturing. Ind. Eng. Chem. Res. 53, 7447–7460. https://doi.org/10.1021/ie402837c.

Mesbah, A., Paulson, J.A., Lakerveld, R., Braatz, R.D., 2017. Model predictive control of an integrated continuous pharmaceutical manufacturing pilot plant. Org. Process Res. Dev. 21, 844–854. https://doi.org/10.1021/acs.oprd.7b00058.

Mirtič, A., Reynolds, G.K., 2016. Determination of breakage rate and breakage mode of roller compacted pharmaceutical materials. Powder Technol. 298, 99–105. https://doi.org/10.1016/j.powtec.2016.04.033.

Olaleye, B., Pozza, F., Wu, C.Y., Liu, L.X., 2019. Population balance modelling of ribbon milling with a new mass-based breakage function. Int. J. Pharm. 571, 118765 https://doi.org/10.1016/j.ijpharm.2019.118765.

Olaleye, B., Wu, C.Y., Liu, L.X., 2020. Impact of feed material properties on the milling of pharmaceutical ribbons: a PBM analysis. Int. J. Pharm. 590 https://doi.org/10.1016/j.ijpharm.2020.119954.

Orehek, J., Teslić, D., Likozar, B., 2021. Continuous crystallization processes in pharmaceutical manufacturing: a review. Org. Process Res. Dev. https://doi.org/10.1021/acs.oprd.0c00398.

Paszke, A., Gross, S., Massa, F., Lerer, A., Bradbury Google, J., Chanan, G., Killeen, T., Lin, Z., Gimelshein, N., Antiga, L., Desmaison, A., Xamla, A.K., Yang, E., Devito, Z., Raison Nabla, M., Tejani, A., Chilamkurthy, S., Ai, Q., Steiner, B., Facebook, L.F., Facebook, J.B., Chintala, S., 2019. PyTorch: an imperative style, high-performance deep learning library. Adv. Neural Inf. Process. Syst. 32, 8024–8035.

Picker, K.M., 2001. Time dependence of elastic recovery for characterization of tableting materials. Pharm. Dev. Technol. 6, 61–70. https://doi.org/10.1081/PDT-100000014.

Qin, S.J., Badgwell, T.A., 1997. An overview of industrial model predictive control technology. NY: American Institute of Chemical Engineers 93, 1971–c2002.

Qin, S.J., Badgwell, T.A., 2003. A survey of industrial model predictive control technology. Control Eng. Pract.

Rao, C.V., Rawlings, J.B., Mayne, D.Q., 2003. Constrained state estimation for nonlinear discrete-time systems: stability and moving horizon approximations. IEEE Trans. Automat. Contr. 48, 246–258. https://doi.org/10.1109/TAC.2002.808470.

Rehrl, J., Kruisz, J., Sacher, S., Khinast, J., Horn, M., 2016. Optimized continuous pharmaceutical manufacturing via model-predictive control. Int. J. Pharm. 510, 100–115. https://doi.org/10.1016/j.ijpharm.2016.06.024.

Reynolds, G., Ingale, R., Roberts, R., Kothari, S., Gururajan, B., 2010. Practical application of roller compaction process modeling. Comput. Chem. Eng. 34, 1049–1057. https://doi.org/10.1016/j.compchemeng.2010.03.004.

Singh, R., Ierapetritou, M., Ramachandran, R., 2012. An engineering study on the enhanced control and operation of continuous manufacturing of pharmaceutical tablets via roller compaction. Int. J. Pharm. 438, 307–326. https://doi.org/10.1016/j.ijpharm.2012.09.009.

Singh, R., Ierapetritou, M., Ramachandran, R., 2013. System-wide hybrid MPC-PID control of a continuous pharmaceutical tablet manufacturing process via direct compaction. Eur. J. Pharm. Biopharm. 85, 1164–1182. https://doi.org/10.1016/j.ejpb.2013.02.019.

Singh, R., Sahay, A., Karry, K.M., Muzzio, F., Ierapetritou, M., Ramachandran, R., 2014. Implementation of an advanced hybrid MPC-PID control system using PAT tools into a direct compaction continuous pharmaceutical tablet manufacturing pilot plant. Int. J. Pharm. 473, 38–54. https://doi.org/10.1016/j.ijpharm.2014.06.045.

Souihi, N., Reynolds, G., Tajarobi, P., Wikström, H., Haeffler, G., Josefson, M., Trygg, J., 2015. Roll compaction process modeling: transfer between equipment and impact of process parameters. Int. J. Pharm. 484, 192–206. https://doi.org/10.1016/j.ijpharm.2015.02.042.

Su, Q., Ganesh, S., Moreno, M., Bommireddy, Y., Gonzalez, M., Reklaitis, G.V., Nagy, Z. K., 2019. A perspective on Quality-by-Control (QbC) in pharmaceutical continuous manufacturing. Comput. Chem. Eng. 125, 216–231. https://doi.org/10.1016/j.compchemeng.2019.03.001.

Sun, C.C., Kleinebudde, P., 2016. Mini review: mechanisms to the loss of tabletability by dry granulation. Eur. J. Pharm. Biopharm. https://doi.org/10.1016/j.ejpb.2016.04.003.

Toson, P., Lopes, D.G., Paus, R., Kumar, A., Geens, J., Stibale, S., Quodbach, J., Kleinebudde, P., Hsiao, W.K., Khinast, J., 2019. Model-based approach to the design of pharmaceutical roller-compaction processes. Int. J. Pharm. X 1, 100005. https://doi.org/10.1016/j.ijpx.2019.100005.

Van Snick, B., Grymonpré, W., Dhondt, J., Pandelaere, K., Di Pretoro, G., Remon, J.P., De Beer, T., Vervaet, C., Vanhoorne, V., 2018. Impact of blend properties on die filling during tableting. Int. J. Pharm. 549, 476–488. https://doi.org/10.1016/j.ijpharm.2018.08.015.